Design and Validation of a Variable Stiffness Three Degree of Freedom Planar Robot Arm

Andrew L. Bernhard
Marquette University

DESIGN AND VALIDATION OF A VARIABLE STIFFNESS THREE DEGREE OF FREEDOM PLANAR ROBOT ARM

by

Andrew L. Bernhard

A Thesis submitted to the Faculty of the Graduate School,
Marquette University,
in Partial Fulfillment of the Requirements for
the Degree of Master of Science

Milwaukee, Wisconsin

December 2023

ABSTRACT
DESIGN AND VALIDATION OF A VARIABLE STIFFNESS
THREE DEGREE OF FREEDOM
PLANAR ROBOT ARM

Andrew Bernhard

Marquette University, 2023

The need exists for robotic manipulators that can interact with an environment having uncertain kinematic constraints. A robot has been designed and built for proof of concept of a passive variable compliance control strategy that can vary joint stiffness to achieve higher performance dexterous manipulation. This novel planar robot incorporating variable stiffness actuators and common industrial controls allows the robot to comply with its environment when needed but also have high stiffness for precise motion control in free space. To perform both functions well, a high stiffness ratio (max/min stiffness) is required. A stiffness ratio up to 492 was achieved.

The robot performance was evaluated with the task of turning a crank to lift a weight despite nominal positioning inaccuracy. The novel variable stiffness robot was able to complete the task faster and with lower constraint forces than a traditional force-controlled stiff robot. The time to complete the task using passive variable stiffness control was twenty-nine times faster with constraint forces less than one fifth those achieved using traditional active compliance control.

TABLE OF CONTENTS

CHAPTER 1

INTRODUCTION

Traditional industrial robot arms are designed for precise absolute positioning control, necessitating high stiffness in the arm structure. When such a robot arm is required to interact with a stiff environment, a small position error resulting in mechanical interference between the robot and the environment generates very large forces. These forces may damage the robot or the environment with which it is interacting.

One strategy to avoid large contact forces is to provide the robot with passive elastic behavior. Elastic behavior is characterized as stiffness or compliance. Along a single axis, increasing stiffness *k* means decreasing compliance *c* and vice versa, and are related as $k = 1/c$. For a particle in planar motion,

$$\boldsymbol{f} = \boldsymbol{K}\boldsymbol{x}$$

$$\begin{bmatrix} f_{\mathrm{x}} \\ f_{\mathrm{y}} \end{bmatrix} = \begin{bmatrix} k_{\mathrm{x}} & k_{\mathrm{xy}} \\ k_{\mathrm{yx}} & k_{\mathrm{y}} \end{bmatrix} \begin{bmatrix} x \\ y \end{bmatrix}$$

where $\boldsymbol{x}$ is displacement from an unconstrained position and $\boldsymbol{f}$ is the forces. The stiffness matrix is $\boldsymbol{K}$, which for the endpoint of a planar robot is a function of configuration and stiffness of the links and joints. Small displacements *x* and *y* can result in high forces when $\boldsymbol{K}$ is large as it is in traditional robots. Designs with more passive elastic behavior have lower values of $\boldsymbol{K}$.

One realization of passive elastic behavior employs the use of serial elastic actuators (SEAs). An SEA has a passive mechanical spring element between a joint positioning motor and the driven link. With compliance built into the joint, geometric

interference between the robot and its environment results in elastic deflection with lower interaction forces. The disadvantage of an SEA structure is the reduction in the precision in positioning an end effector, especially with respect to structural vibration in the robot and when manipulating objects of uncertain weight. With an SEA device the passive stiffness is not controllable, and the maximum stiffness of the robot is limited by the stiffness of the spring element.

An alternative to an SEA which offers many advantages is a variable stiffness actuator (VSA). A variable stiffness actuator has a range of stiffness values that can be achieved. With a robot arm constructed with VSA joints, it is possible to both control robot endpoint compliance in different directions and control endpoint position [1].

1.1 Prior Work: Existing VSA Designs

Many VSA designs have been produced, each typically with their own acronym to identify some unique feature they possess. In general though, there are two main classes of VSA joint architectures [2]. One class of designs uses two motors in an antagonistic configuration. The other class uses two independent motors, one for joint position and another for adjusting the stiffness. Independent stiffness adjustment designs may use a spring with adjustable preload, or a spring with an adjustable active length. Springs may be torsional, beam (lever), or longitudinal. Desired qualities in a VSA are low weight, compact size, high torque rating, and fast actuation of stiffness adjustment. Depending on the specific application, these qualities may be weighted differently in importance with respect to overall system performance and the type of task to be performed. For instance, throwing a dart [3] or hammering a nail [4] could require a rapid change in stiffness at the beginning or end of the motion, while interacting along a kinematically constrained path requires high stiffness along the path but high compliance

along the direction of the constraints. Meeting such a goal is not done with a single joint, but can be accomplished with a robot arm consisting of multiple VSA joints working together.

Figure 1.1 shows a VSA of the antagonistic motor type. It contains two motors M1 and M2, each connected to the output link via nonlinear springs whose stiffness increases with increasing deflection. When both motors move to lengthen the springs (increasing θ_1 and θ_2), the stiffness of the link increases. Differential motion of the motors results in a change of the link angular position θ_3. Such designs are limited in their maximum stiffness that can be achieved by the stiffness of the springs at their maximum allowed extension. Another limitation is imposed by the high energy expenditure required to hold high stiffness by stretching the springs when maintaining a position.

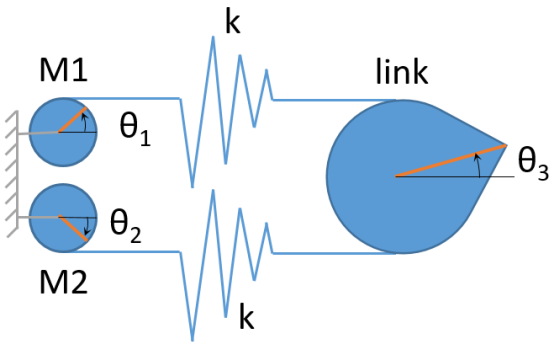

Figure 1.1:Antagonistic motor VSA with nonlinear springs. Motors M1 and M2 can be driven independently to change link position and/or stiffness.

Another type of VSA is shown in Figure 1.2 which contains a variable spring element in series between the driving joint motor M1 and the link. Motor M2 can be a smaller motor which changes the stiffness characteristic of the spring. Changing the stiffness can be implemented in a variety of ways such as varying spring tension,

changing a pivot point location, or changing the loading point of a lever or beam type spring.

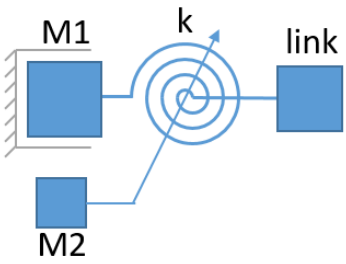

Figure 1.2: VSA with one actuator to position link and a second actuator to adjust spring stiffness independently of link position.

Performance specifications for different existing VSA designs are listed in Table 1. Antagonistic designs generally have faster full stiffness variation times, but lower maximum torque, stiffnesses, and stiffness ranges. The published data for the various designs do not always make it clear whether performance specifications are theoretical or experimentally measured. For example the AwAS-II is reported to have an infinite maximum stiffness and zero minimum stiffness, but these must be assumed to be theoretical limits as any real physical device would have a finite maximum stiffness.

Table 1: Performance specifications of existing VSA designs.

Performance Criterion	Unit	VSA-CUBE [5]	BAVS [6]	FAS [7]	VSA-HD [8]	AwAS-II [9]	FSJ [10]
Full Stiffness Variation Time	ms	180	14	29	400	2000	330
Maximum Torque	Nm	3	8	4.9	14	80	67
Maximum Stiffness	Nm/rad	14	146.6	36	8360	Inf	826
Minimum Stiffness	Nm/rad	3	3.9	1.8	0.38	0	52.4
Maximum Deflection with max. stiffness	Degree	8.6	0	1.5	0.8	17	3
Maximum Deflection with min. stiffness	Degree	15.8	18.2	30	60	0	15
Mass	kg	0.26	0.75	3.9	1.7	1.4	1.41
Type: Antagonistic (A) or Independent Stiffness Adjustment (ISA)		A	A	A	ISA	ISA	ISA

While there are many examples of VSA designs in the literature, few have been implemented in a full robot system. One such is the Cube-Bot which was demonstrated to perform the task of drawing a circle on an uneven horizontal surface [11] and implementing a search pattern to complete an assembly task [12]. One other example is a three degree of freedom planar manipulator with two hybrid-type VSAs used to perform an insertion assembly task [13]. No prior system has demonstrated a bilaterally constrained manipulation task using passive compliance control.

1.1.1 Antecedent of This Project: Central Shaft Beam-Contactor Flexure

One aspect of the present project is the refinement of a previous beam flexure design which used contactors that swept along a profiled beam flexure to vary joint stiffness [14]. In this previous design, shown in Figure 1.3 below, motion was transmitted from the drive motor to the beam flexure. Because the shaft is relatively thin, a large amount of unwanted compliance is added to the system. Additionally, because the high stiffness setting placed the contactors in a position radially close to the driving shaft, very large forces on the contactors were required in order to transmit high torque. To achieve

higher maximum stiffness and reduce forces on the contactors, a different flexure geometry and a different type of actuator transmission are needed.

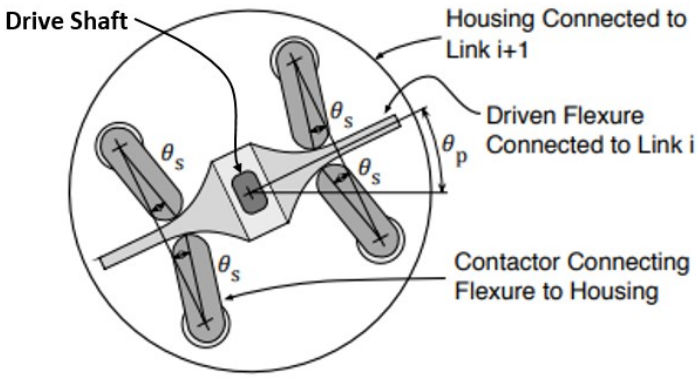

Figure 1.3: Previous generation beam flexure VSA design. Maximum stiffness performance suffered from compliance in the central drive shaft and large force loads required to transmit torque at high stiffness setting. [14]

1.2 Approach

The robot arm described in this thesis is able to perform a kinematically constrained task with a high degree of dexterity using a passive variable compliance control strategy. The arm is a planar mechanism and performs the task in a vertical plane.

With the passive variable compliance control strategy, a priori knowledge of the task is used to compute a path through the combination of compliance and position task space. The robot endpoint compliance in the x and y directions is a function of each joint's individual compliance and the kinematic configuration of the arm, both of which are simultaneously controlled in real time throughout the task execution. For known joint compliances c_i, the particle planar translational endpoint compliance is calculated as

$$\boldsymbol{C} = c_1\boldsymbol{t}_1\boldsymbol{t}_1^T + c_2\boldsymbol{t}_2\boldsymbol{t}_2^T + \cdots + c_n\boldsymbol{t}_n\boldsymbol{t}_n^T \qquad (1)$$

where $\boldsymbol{t}_i$ is a planar motion twist for each joint determined by

$$\boldsymbol{t}_i = \boldsymbol{r}_i \times \boldsymbol{k}$$

where $\boldsymbol{r}_i$ is the position vector of each joint relative to the end effector, and $\boldsymbol{k}$ is the unit vector perpendicular to the plane of the arm. For the 2D planar case, the arm requires three joints to fully control the 2D translational compliance of the endpoint at any position in the task space [1]. In conventional terms, a robot arm with three joints is a three degree of freedom (3DOF) system, which is why the robot described in this thesis is referred to as a 3DOF arm, even though the spatial degrees of freedom are reduced to two when applying the passive compliance control method.

An example of a constrained manipulation task where variable impedance control is advantageous is shown in Figure 1.4 below. Here a planar 3R manipulator with variable stiffness at each joint pushes a load across a surface and into a wall. The two-dimensional Cartesian compliance of the manipulator is visually represented by a compliance ellipse. The vertical and horizontal compliance c_y and c_x are represented by the major and minor axes of the ellipse, respectively. The series of ellipses correspond to the endpoint compliance at different points in the manipulator end-effector path. Throughout the task, a constant high compliance c_y in the vertical direction minimizes interaction forces with the horizontal surface. In the horizontal direction, compliance c_x is initially low so that the commanded motion moves the load, then is increased as the manipulator approaches the wall to minimize forces on the robot provided by the wall.

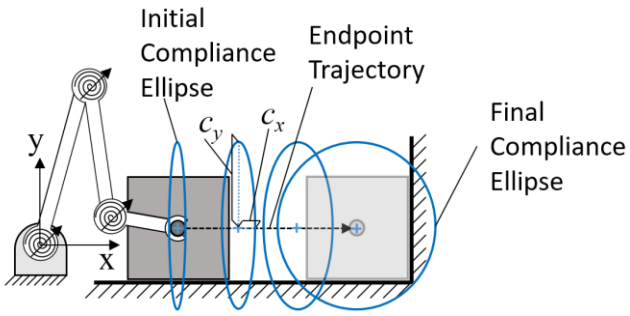

Figure 1.4: Example of a kinematically constrained manipulation task. Endpoint compliance changes with task progression to reduce reaction forces from contacting fixed environmental constraints.

1.2.1 Specific Planar Robot Design Objectives

The primary objective of this project is to design a 3DOF planar robot arm that is able to reliably perform a constrained manipulation task. Desired qualities of the links are high stiffness (to make the VSAs the dominating compliant elements in the system) and low weight. A 3DOF planar arm utilizing a VSA for each joint can control Cartesian position and compliance of an end effector at any point in its compliance dexterous workspace (locations that can be reached by the end of the second link). Determining the available workspace of end-effector compliance and position as well as planning a task path through that workspace is covered in [15, 16].

1.2.2 Specific VSA Design Objectives

Controlling the compliance ellipse throughout a task such as shown in Figure 1.4 requires the use of a VSA at each joint. The VSA is designed to independently control both joint position and joint stiffness. The design is expected to provide a wide range of commanded stiffness values to maximize the compliance and position workspace. Position feedback of the joint angle is used for control and data collection. In addition, angular deflection from equilibrium at the joint is measured to protect against overload

conditions. The angular deflection measurement also provides a means of measuring the joint stiffness if a known torque is applied.

The design goals for the VSA mechanism are summarized in Table 1 below. A high stiffness ratio (maximum stiffness to minimum stiffness) is desired. Ideally, the mechanism has high stiffness for precise positioning when unconstrained, and a low stiffness when kinematically constrained.

Table 2: VSA Design Goals

Stiffness Ratio	> 1000
Time to change from minimum to maximum stiffness	< 200 ms
VSA Mass	< 1.0 kg

A high stiffness range is realized by changing the location where the driving element for stiffness adjustment of the joint (each contactor) is in contact with the position driven element (the flexure) as shown in Figure 1.5 below. In the previous design utilizing the central shaft structure (Figure 1.3), the experimentally measured stiffness ratio was 55, while simulations showed an expected stiffness ratio of 100 [14]. For the current design, the targeted stiffness ratio is 1000 or greater.

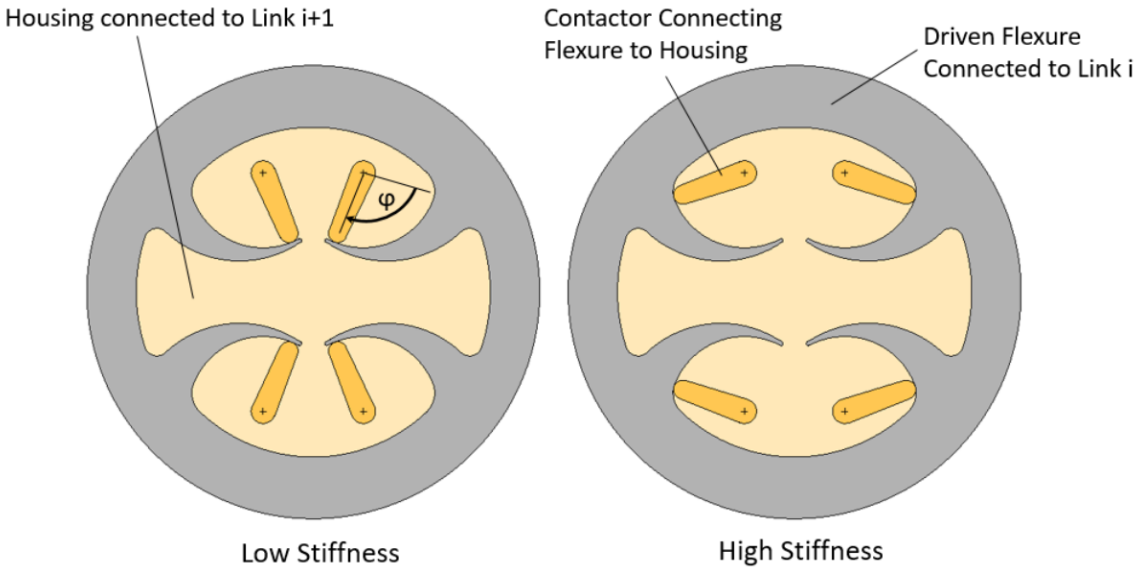

Figure 1.5: New VSA structure at low and high stiffness configurations.

Figure 1.6 shows how a small range of zero stiffness is achieved when the contact forces are directed through the center of the joint thus unable to provide any counteracting torque to joint rotation. In practice, once there is a small deflection, the flexure starts to push against the contactor resulting in a still small but nonzero stiffness.

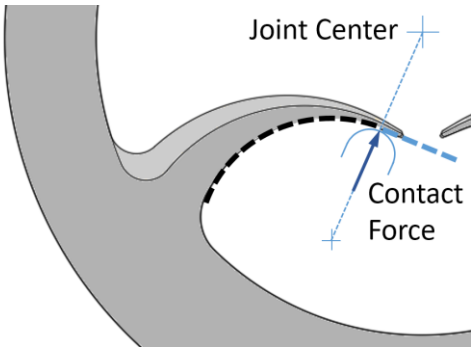

Figure 1.6: Zero stiffness realization. When contactors point toward center of VSA, the contact force from each contactor passes through the joint center resulting in possible unconstrained motion about the joint center yielding a small range of motion with zero stiffness.

In addition to the ability to set compliance within a wide range, it was desired to be able to change the compliance quickly throughout that range, from maximum to

minimum compliance or vice versa. Being able to change compliance quickly allows greater freedom in programming motion tasks without being limited by the speed of the compliance actuation. A goal of 0.2 seconds actuation time to sweep between extremes of the stiffness range was chosen.

A compact design was desired to yield an actuator that could be incorporated into a robot arm comparable in length to an adult human arm. A lightweight design maximizes the load carrying capability of the robot.

1.3 Overview

This thesis describes: 1) the design of a novel 3DOF VSA-driven robot, and 2) its ability to perform a kinematically constrained task quickly and reliably.

The robot manipulator system is described in Chapter 2. The robot manipulator system consists of a 3-joint planar robot arm with a VSA at each joint and the robot controller. Chapter 3 describes the structure and functionality of the VSA joints and contains supporting analytical and experimental performance data. The robot system performance was evaluated with the trial task of turning a crank to lift a weight. Chapter 4 shows that passive compliance control of the robot (made possible by the variable stiffness actuators) is able to perform the crank turning task 29 times faster and with much lower constraint forces than a more traditional active compliance control approach that lacks VSA functionality.

CHAPTER 2

ROBOT SYSTEM DESIGN

The robot system consists of the manipulator mechanical structure and the electric control system.

The manipulator overall mechanical structure is presented in Section 2.1. Section 2.2 describes the design of the links in the manipulator and the FEA simulations used to predict their stiffness. Section 2.3 discusses the actuators selected to drive the link positions and presents an overview of the electric control system that provides synchronous motion and data collection.

2.1 Manipulator Design

Three VSA assemblies are incorporated into a 3 revolute joint planar robot arm as shown in Figure 2.1 below. The global coordinate system used for the manipulator is fixed at the center of the first joint. The first joint angle θ_1 is defined relative to the horizontal global x axis. Joint angles θ_2 and θ_3 are each defined relative to the angle of their respective preceding link. Each VSA joint has a motor to actuate the stiffness selection mechanism and a harmonic drive motor to control the joint position.

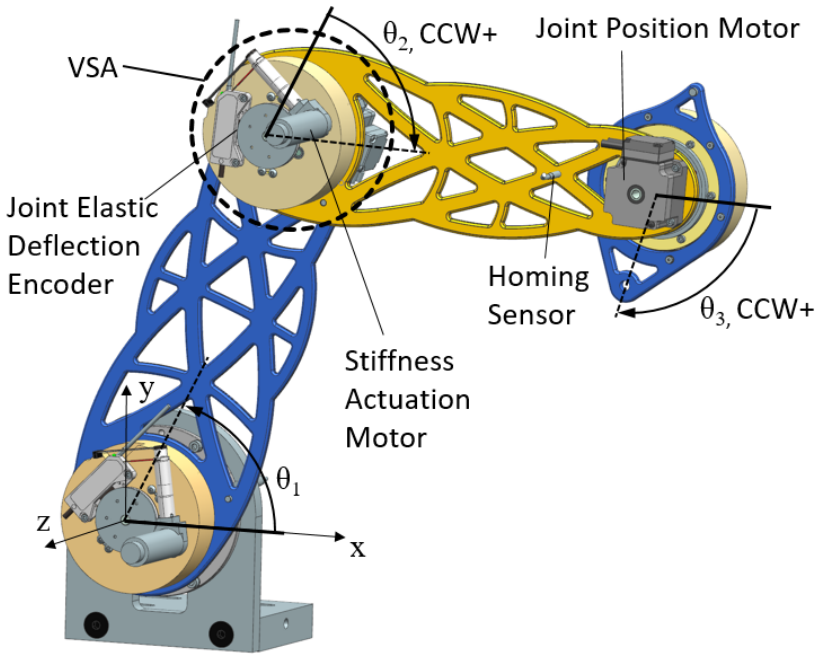

Figure 2.1: 3R Robot arm assembly with coordinate system definitions. Each VSA joint has a separate motor for controlling joint stiffness and joint position.

The links for the robot arm provide structures for mounting the input and output sides of each VSA joint. The links are designed to be lightweight yet stiffer than the stiffest setting of each VSA so that the compliance of the VSA dominates the system. The lengths were chosen to mimic adult anthropomorphic dimensions.

The robot arm was designed to support a maximum load of 6 kg when fully extended with joints at their maximum stiffness. The maximum moment is seen when supporting a load in the fully outstretched horizontal position of the arm. At lower stiffness settings, more deflection can be accommodated, but the load rating is decreased. The limiting factor is stress in the flexures of the VSA joints. Each joint was designed to allow up to 13mm (1/2”) of deflection at the end effector with the arm fully outstretched at the minimum stiffness setting, without over-stressing the flexure.

Physical attributes of the robot system are summarized in Table 3 below. Each link length, link mass, and distance of each link center of mass (COM) relative to its

respective link's rotation (joint) axis are used along with the VSA masses and joint positioning motor masses in accounting for the effects of gravity on the endpoint position. Gravity compensation was included in the trajectory planning computation [16].

Table 3: Robot Physical Parameters

Parameter Description	Symbol	Value	Units
Link 1 Length	L_1	0.32	m
Link 2 Length	L_2	0.3	m
Link 3 Length	L_3	0.08	m
Link 1 Mass	m_{L1}	0.448	kg
Link 2 Mass	m_{L2}	0.376	kg
Link 3 Mass	m_{L3}	0.08975	kg
Link 1 COM distance	b_1	0.156	m
Link 2 COM distance	b_2	0.136	m
Link 3 COM distance	b_3	0.0067	m
VSA Mass	M_{VSA}	1.0	kg
Joint Position Motor 2 Mass	M_2	1.2	kg
Joint Position Motor 3 Mass	M_3	0.4	kg

2.2 Link Design and FEA Simulation

Finite element analysis was performed to ensure that the links are both very stiff and very light. The numerical analysis indicated that the maximum deflection under the rated load for the first link is 0.00316 inch; whereas, a deflection of .00615 inch results when the rated load is applied and the shoulder joint is at its stiffest setting. This link stiffness to joint stiffness ratio is typical in the robot. The links are approximately twice as stiff as the VSA when the VSA is at its maximum stiffness setting.

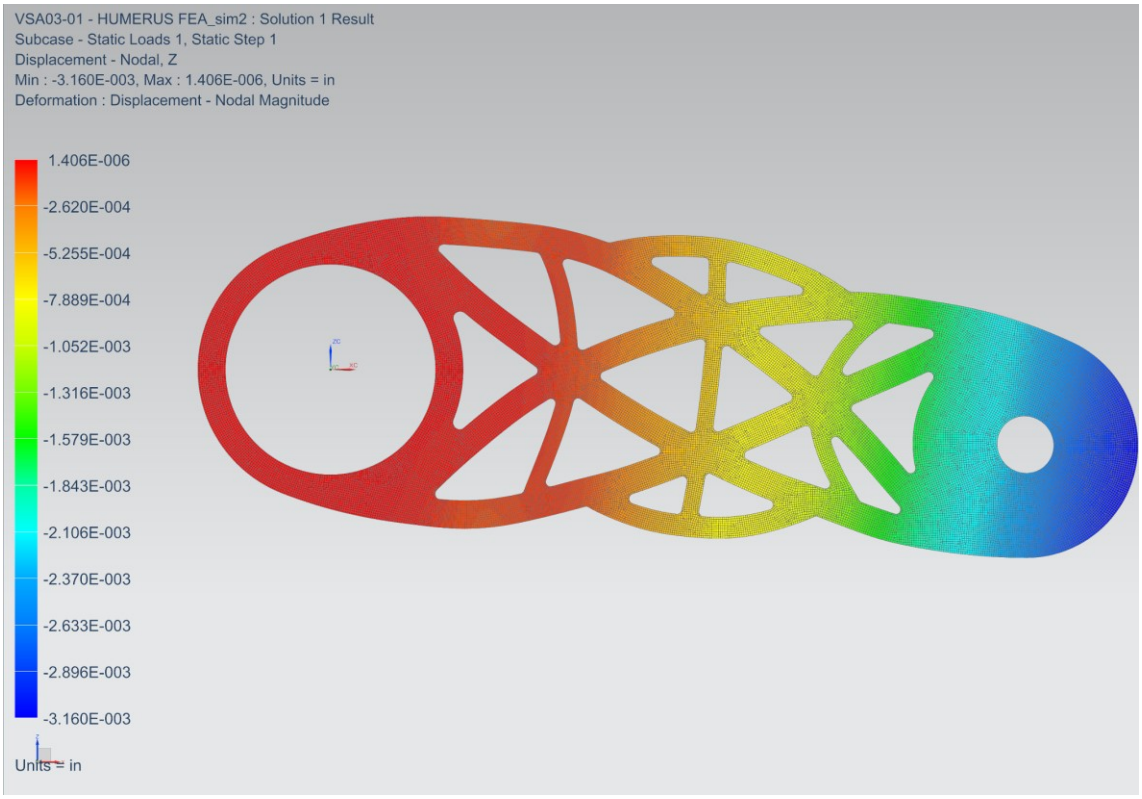

Figure 2.2: FEA displacement results for first link at rated load. Max deflection is .003".

2.3 Robot Actuation and Control

Robot position and compliance are controlled by a system consisting of motor drives, power supplies, sensors, I/O modules, and a controller. National Instruments software and hardware are used to execute a pre-programmed motion and compliance profile by commanding synchronous motion of the six motors (3 for joint position and 3 for compliance.)

2.3.1 Main Control

The motor drives are controlled and sensors are read by a National Instruments compactRIO-9064 (cRIO) controller. Two additional modules are installed in the c-RIO for the base robot system: a digital I/O module for reading joint deflection encoders and a CAN module for bidirectional communication with the motor drives. The cRIO is

powered by a 24V DC power supply. The overall control structure is illustrated in Figure 2.3.

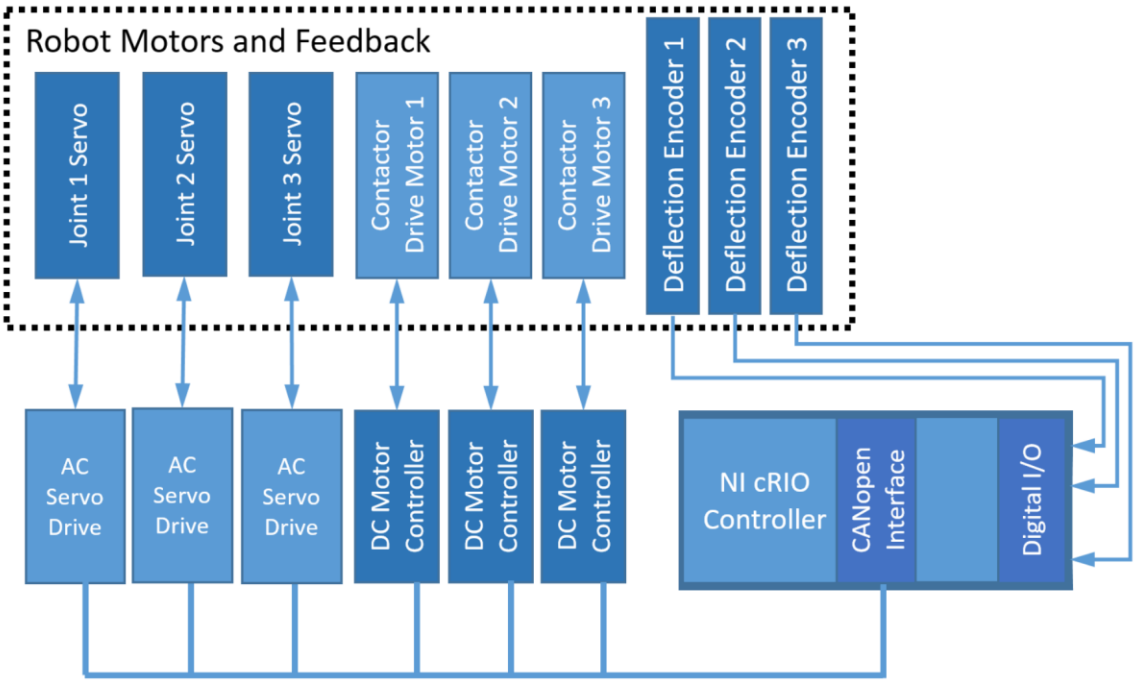

Figure 2.3: Electrical and Control system diagram. All components link to CompactRIO controller.

Each motor drive receives commands and sends status and other data to the c-RIO controller via a CANopen industrial communication network. All drives are connected in parallel on a bus and uniquely addressed. The CANopen protocol enables synchronous motion among all the motor drives and can communicate at a speed of up to 1 Mbit/s.

2.3.2 Motion Actuation and Control

Each joint contains a harmonic drive actuator to drive the link position. The motor in each harmonic drive actuator is a three phase permanent magnet AC servomotor. Each motor is controlled by a Kollmorgen AKD AC servo drive. While many AC servo drives are commercially available to control such motors, this particular model was chosen due

to its compatibility with the CANopen industrial communication protocol and the flexibility of using additional encoder inputs.

Each motor has an incremental encoder to close a position feedback loop with its respective drive. A homing routine for each joint uses inductive proximity sensors triggered by a reference target on each link to set the zero position for each encoder.

2.3.3 Stiffness Actuation and Control

DC motor control boards from Maxon were used to control DC gearmotors for setting the joint stiffness. These motor control boards use the CANopen industrial communication protocol which prompted the selection of the other servo drives in the system. With all drives on the same network, motion can be synchronously commanded for all six drives. Each stiffness actuation motor is equipped with an incremental encoder for position feedback and is homed with an inductive proximity sensor.

Joint deflection from equilibrium is measured directly with a 19-bit absolute encoder which gives a resolution of 6.87e-4 degrees (12.0 μrad). A digital I/O module in the compactRIO is interfaced to the absolute encoders through RS-485 transceiver modules. The encoders communicate using the BISS-C serial protocol. For the compactRIO to read data from the encoders, a LabVIEW VI was created which makes use of the compactRIO's FPGA to transmit clock pulses to the encoders and receive the bits transmitted by the encoder. The flexure deflection measurement triggers a fault that stops robot motion if the deflection exceeds the limit for the flexure.

2.4 Summary

The robot is designed and constructed to achieve dexterous planar manipulation by simultaneously controlling position and passive compliance at the end effector. The links give the robot a stiff structure for precise position control when motion is

unconstrained. The VSA joints make passive compliance control possible when motion is constrained. The electrical system utilizes standard industrial motion control hardware to integrate the joint position and stiffness actuation motors into a complete robot system. The enabling technology for robot dexterous manipulation is the novel VSA design which is described in depth in the following chapter.

CHAPTER 3

VSA DESIGN AND PERFORMANCE

The variable stiffness actuator (VSA) is the component which makes the manipulator capable of achieving a large range of endpoint compliance. This chapter describes the VSA design in greater detail including its structure. The VSA has two essential functions: positioning the robot joint angle and adjusting the joint stiffness. The simulations and tests used to verify its performance are also described.

The overall geometry and functionality of the VSA device are described in Section 3.1. Section 3.2 first gives an overview of the basic concept for transmitting motion from the joint positioning actuator using a beam flexure design. The means of controlling stiffness through the positioning of contactors along the length of the flexure beams is then described. A series of section views are presented which walk through layers of gearing and structural components. An analytical model relating desired stiffness characteristics with contactor location along the flexure beams is presented in Section 3.3. Numerical simulation was used to design the flexure geometry that meets the desired stiffness characteristics. Section 3.4 presents experimental verification of the large range in elastic behavior obtained using the fabricated VSA.

3.1 VSA Overall Geometry

An exterior view of the fully assembled VSA shoulder joint is shown in Figure 3.1. The VSA functions as a motor and an elastic transmission which transmits motion from the harmonic drive actuator (6) rigidly attached to link i and elastically connected to link i+1 (5).

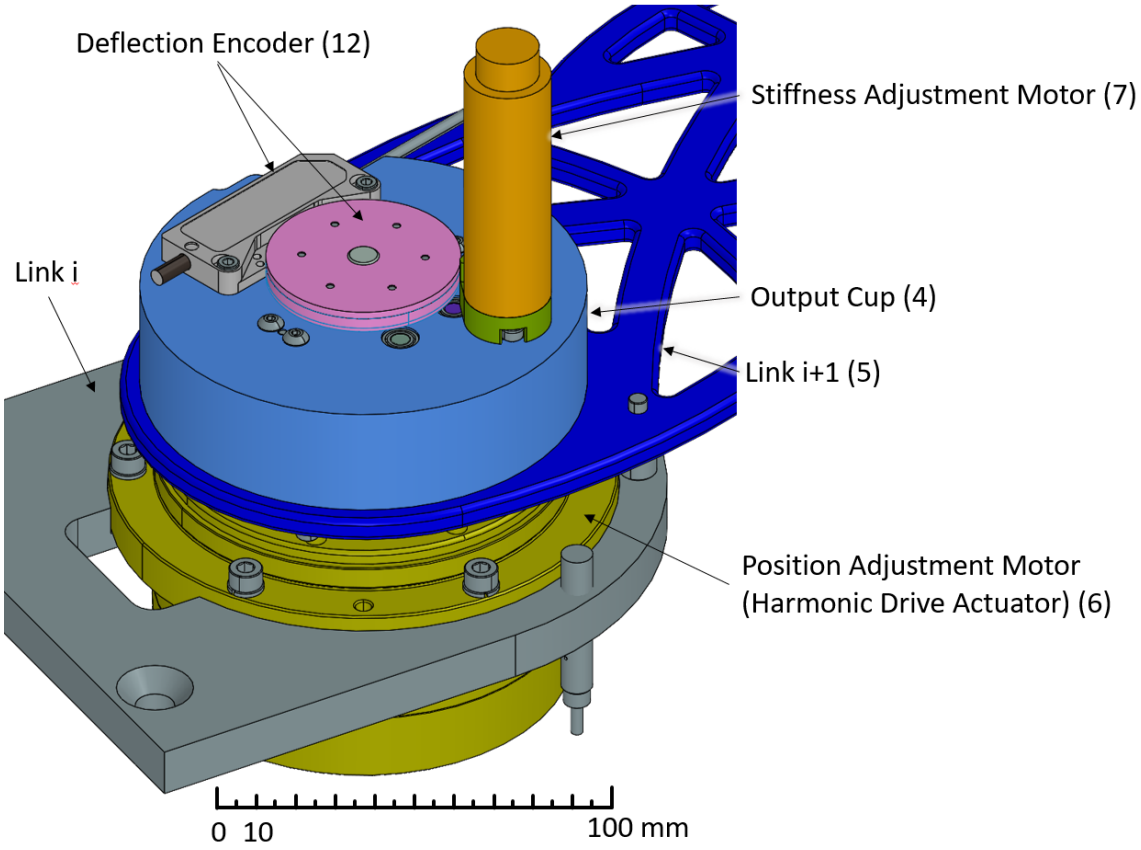

Figure 3.1: Fully assembled shoulder VSA joint

Figure 3.2 shows the VSA mechanism color coded with yellow (input) attached to link i and blue (output) attached to link i+1. The harmonic drive actuator body is a fixed reference for joint motion and is attached to the distal end of the previous link (or base mount in the case of the shoulder). The input side drive flange and output side output cup are coupled by a thin section ball bearing (3) providing one degree of freedom between adjacent links. A redundant central shaft bearing (22) serves the same function, increasing the rigidity of the assembly. All parts in the VSA listed in Table 4 are illustrated in the figures that follow.

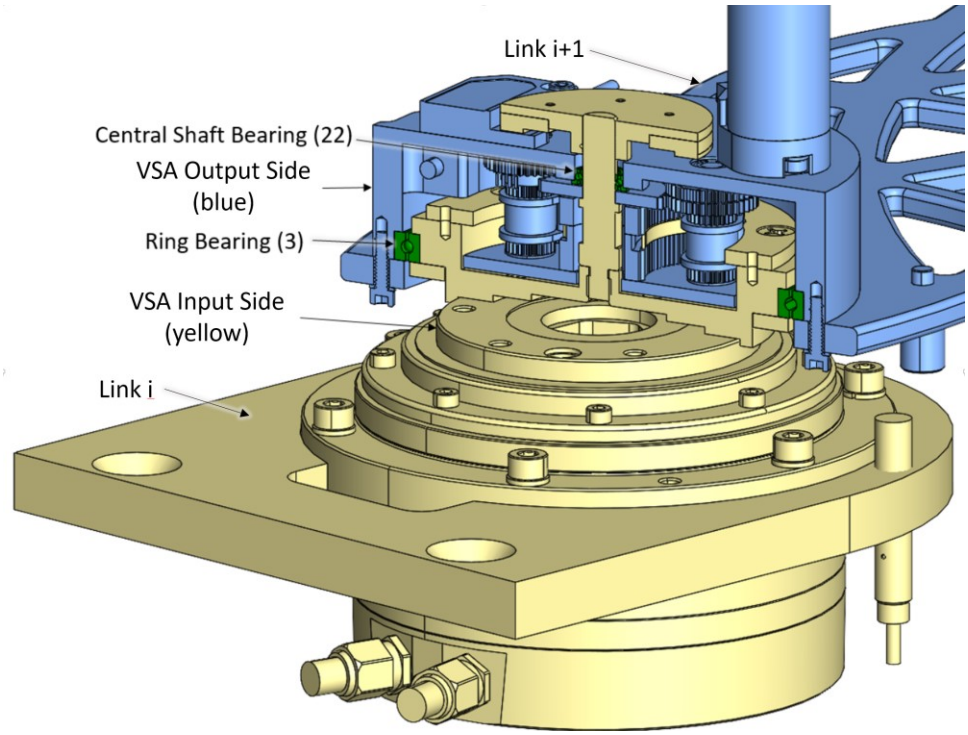

Figure 3.2: Section view of VSA. A harmonic drive actuator drives the input side (yellow: link i) and imparts force through a flexure to the output side (blue: link i+1) which is connected to the next link structure. The bearings fixing all degrees of freedom except rotation about the joint axis are shown in green.

Table 4: VSA key component list

ID	Component Name		ID	Component Name
1	Drive Flange		13	Ring Gear, Bottom
2	Flexure		14	Needle Bearings
3	Ring Bearing		15	Sun Gear
4	Output Cup		16	Planet Gear
5	Link i+1		17	Ring Gear, Top
6	Harmonic Drive Actuator		18	Transfer Gear
7	Stiffness Adjustment Motor		19	Idler Transfer Gear
8	Central Shaft		20	Contactor Drive Gear
9	Contactor Drive Shaft		21	Inductive Proximity Sensor
10	Bottom Plate		22	Central Shaft Bearing
11	Ring Bearing Retainer		23	Bottom Plate Screws
12	Deflection Encoder			

Figure 3.3 is a section view of the bottom layer of the VSA mechanism. The drive flange (1) is fastened to the harmonic drive output. The ring bearing (3) shown in Figure 3.2 is secured to the drive flange with the ring bearing retainer (11). The outer race of the ring bearing is clamped by the output cup and driven link i+1 (5) which are fastened together. The ring bearing constrains all degrees of freedom between the drive flange and output cup except for rotation about the joint axis.

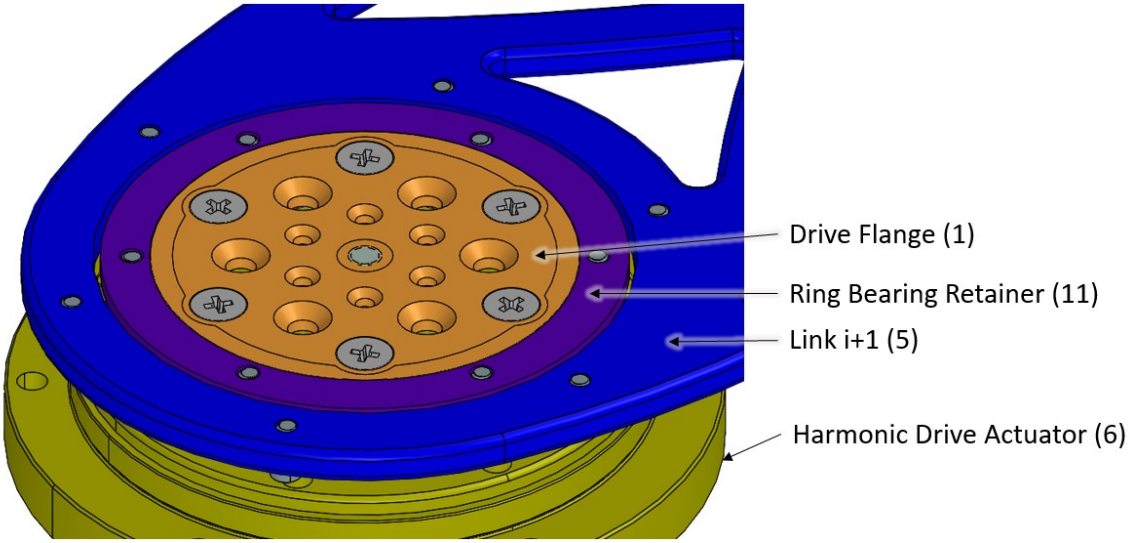

Figure 3.3: VSA joint angle driver. Drive flange is mounted to harmonic drive actuator. The ring bearing isolates link i+1 from the harmonic drive attached to link i.

3.2 Stiffness Variation Functionality

The design of the variable stiffness function of the VSA device is centered on the concept of a cantilever beam flexure which, when loaded at its tip, exhibits low stiffness, and when loaded at its base, exhibits high stiffness. The VSA design has an elastic flexure element which can be loaded at different points along its length by a set of rolling contactors. The contactors are made of needle bearings so they can move along the flexure without sliding friction, and forces are transmitted back to the contactor drive shafts and main body of the VSA.

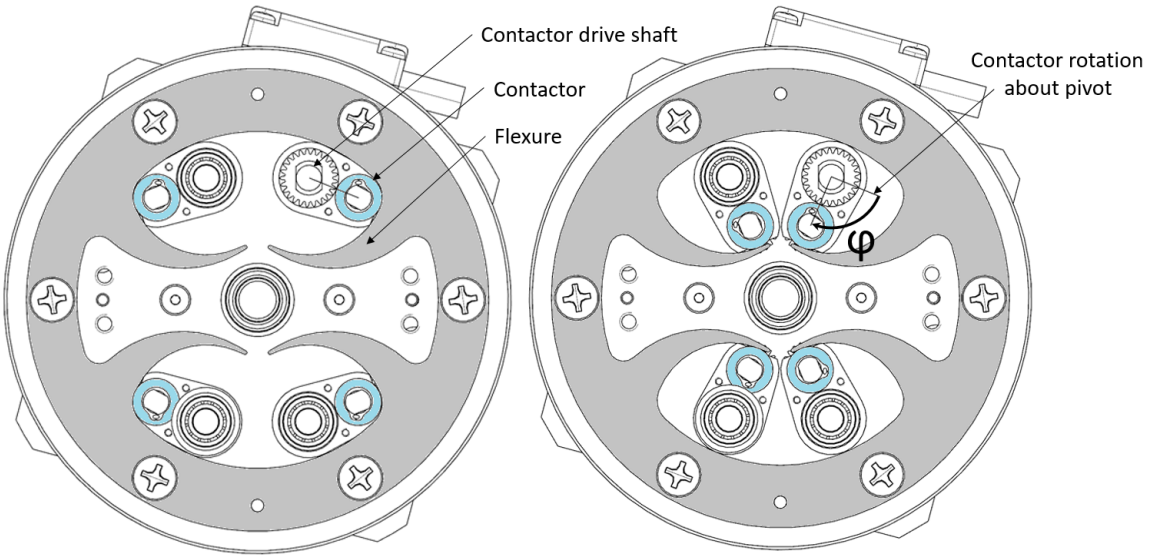

Figure 3.4: VSA showing flexure (gray) and contactors (blue). Contactor position (angle φ) is shown for maximum stiffness (left) and minimum stiffness (right).

Figure 3.4 shows a simplified view of the VSA with two different contactor configurations. The configuration on the left corresponds to joint maximum stiffness, and the one on the right corresponds to joint minimum stiffness. Four contactors and mating flexure beams are used to enable bidirectional operation of the VSA and to provide symmetric loading. The contactor bearings are highlighted in blue. Figure 3.5 shows a partially assembled VSA with a clear view of one of the rolling contactor assemblies.

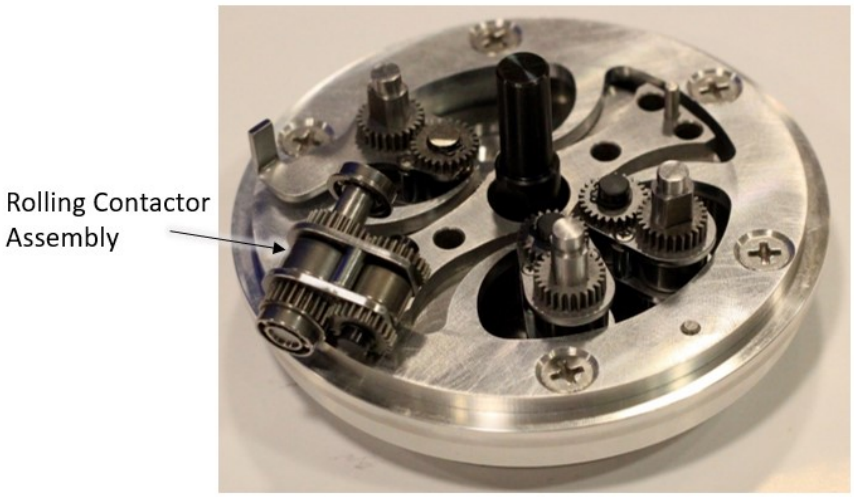

Figure 3.5: Partially assembled VSA showing rolling contactor subassembly removed from the VSA. Transfer gears linking contactor motions not shown.

The contactor positioning system is responsible for moving all four contactors simultaneously to effect a change in the joint stiffness. The system elastically transmits the motion of the harmonic drive actuator (6) to the link via the flexure and contactors.

Figure 3.6 is a section view in which the various layers of the VSA are visible. The contactor positioning system is located between the bottom plate (10) and the output cup (4). A central shaft (8) is threaded into the drive flange (1) and passes through a bearing (22) at the top of the output cup. The deflection encoder codewheel (12) is affixed to the central shaft to allow measurement of the relative angular position between the drive flange and the output cup, measuring the deflection of the flexures. The sequence of section views that follow provide a layer by layer functional description of the VSA geometry.

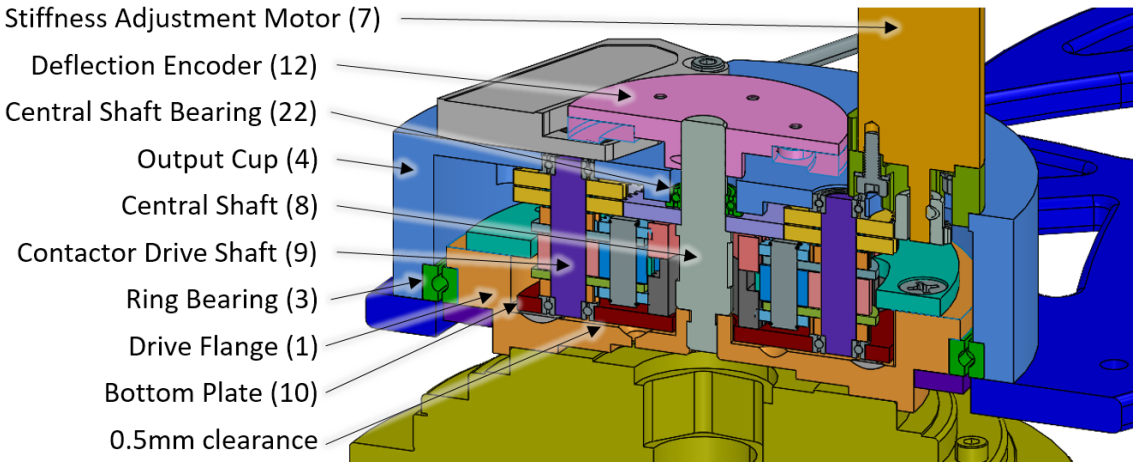

Figure 3.6: Sectioned CAD rendering of VSA mechanism with visible layers.

Figure 3.7 shows a section view of the VSA layer containing the flexure (2) and rolling contactors. To reduce friction and wear in the drive system, the contactor drive system employs rolling needle bearing contactors (14). Each contactor assembly drive shaft (9) is supported by a ball bearing at the top and the bottom, as shown in Figure 3.6. One bearing provides near frictionless support from the bottom plate (10) and the other provides near frictionless support from the output cup (4). A 0.5 mm clearance between the bottom plate (10) and the drive flange (1) allows frictionless relative motion between the two.

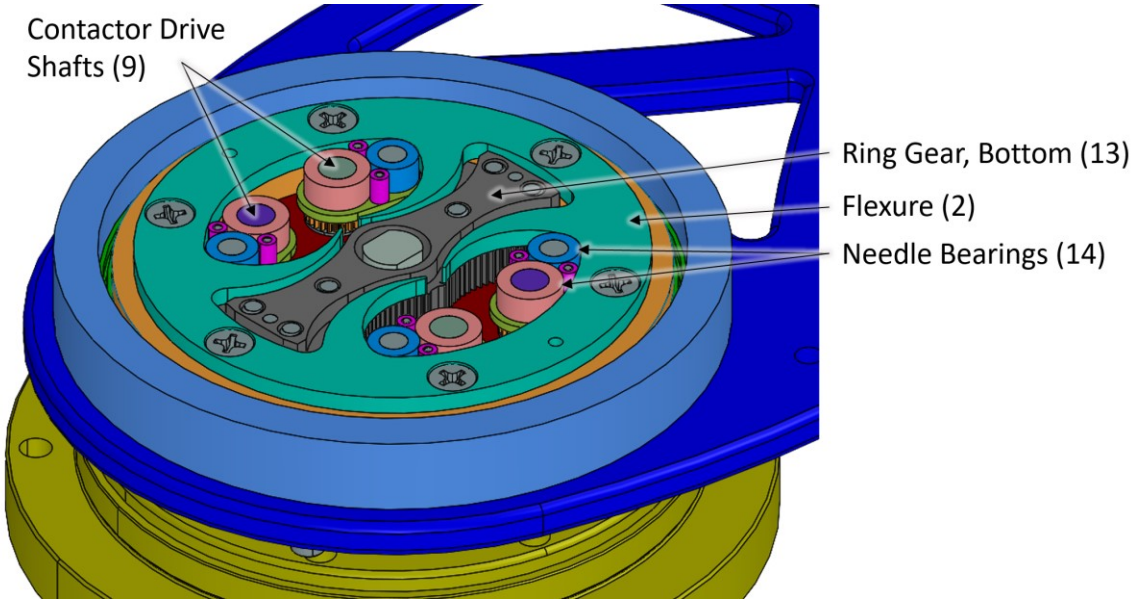

Figure 3.7: VSA flexure and contactors.

The location at which the contactor interacts with the flexure is determined using a planetary gearing system. The planetary gearing provides a very high stiffness means of controlling the angular position of the contactors. Using this system, each contactor is supported both above and below the loading point at the flexure. The layers providing contactor support are shown in Figure 3.8 and Figure 3.9.

The ring gear of the planetary gear system is a two-piece component. The flexure fits in a pocket between the top half of the ring gear (17 in Figure 3.8) and bottom half of the ring gear (13 in Figure 3.9). The ring gear bottom is fastened to the bottom plate (10). The planet gears (16) are coaxial with the needle bearings that touch the flexure. The sun gears (15) are keyed to the contactor drive shafts (9). The bottom plate supports one end of the contactor drive shafts and holds the contactor drive system together when fastened to the output cup with four screws (23) that pass through clearance holes in the output cup and top and bottom ring gears. Dowel pins precisely locate the ring gear sections on the output cup and bottom plate.

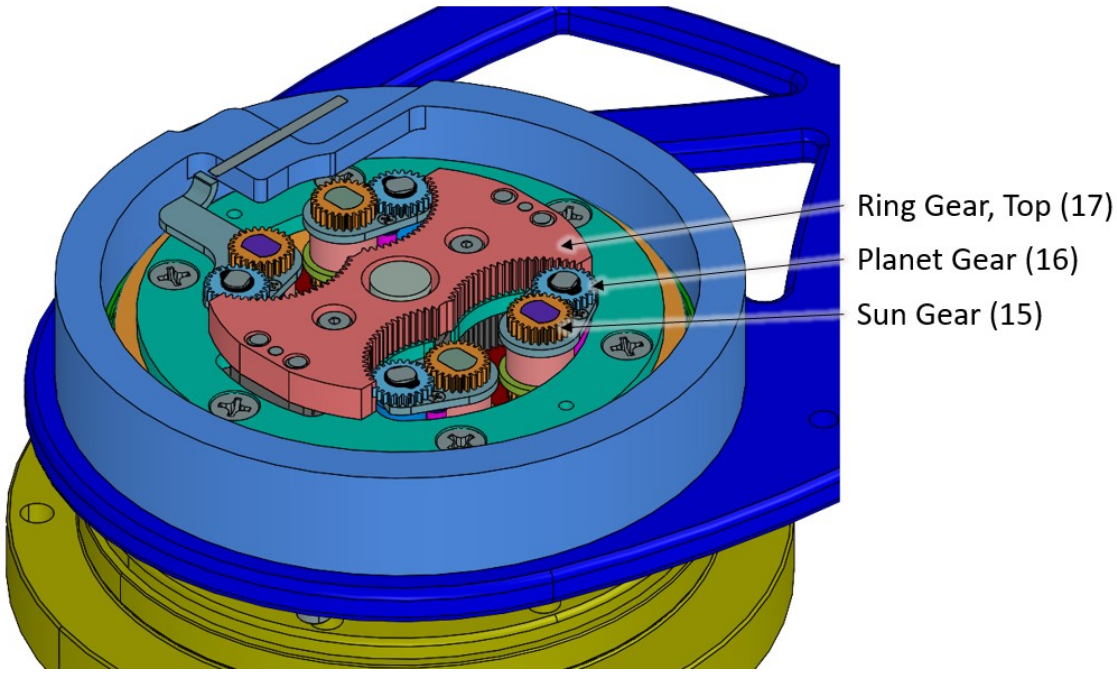

Figure 3.8: Upper level of contactor drive planetary gearing.

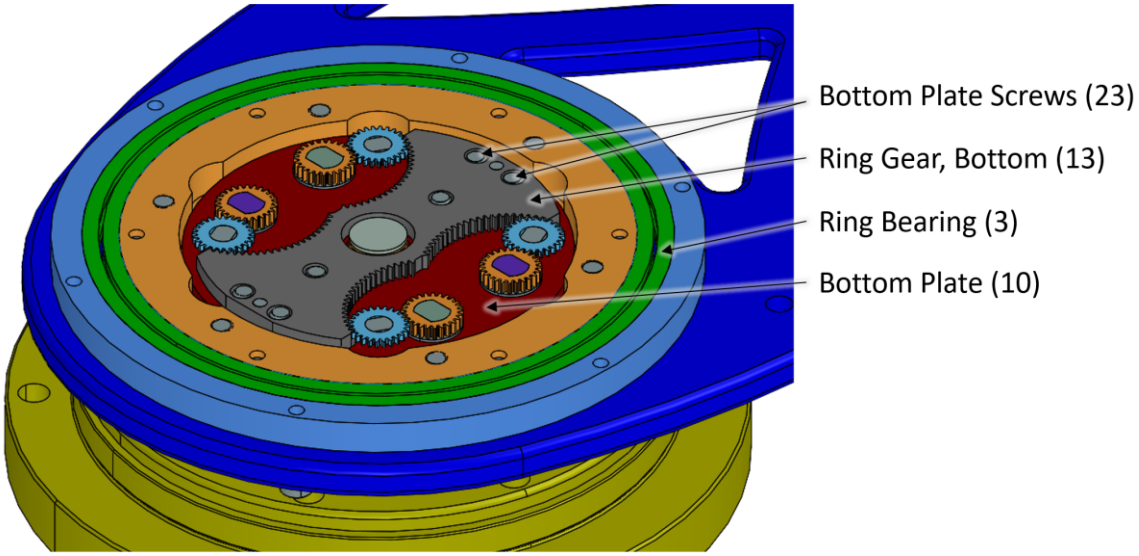

Figure 3.9: Bottom level of contactor drive planetary gearing.

Figure 3.10 and Figure 3.11 show the transfer gear layers above the planetary gearing. Figure 3.10 shows the top layer of transfer gearing which provides even symmetry of contactor motion to adjacent contactor pairs. The transfer gears (18) are keyed to the contactor drive shafts (9) and rotate when driven by the stiffness adjustment

motor (7 in Figure 3.1) via the contactor drive gear (20). Figure 3.10 also shows the inductive proximity sensor (21) mounted in the output cup. It senses a target on one of the contactor assemblies and is used for homing the contactor position.

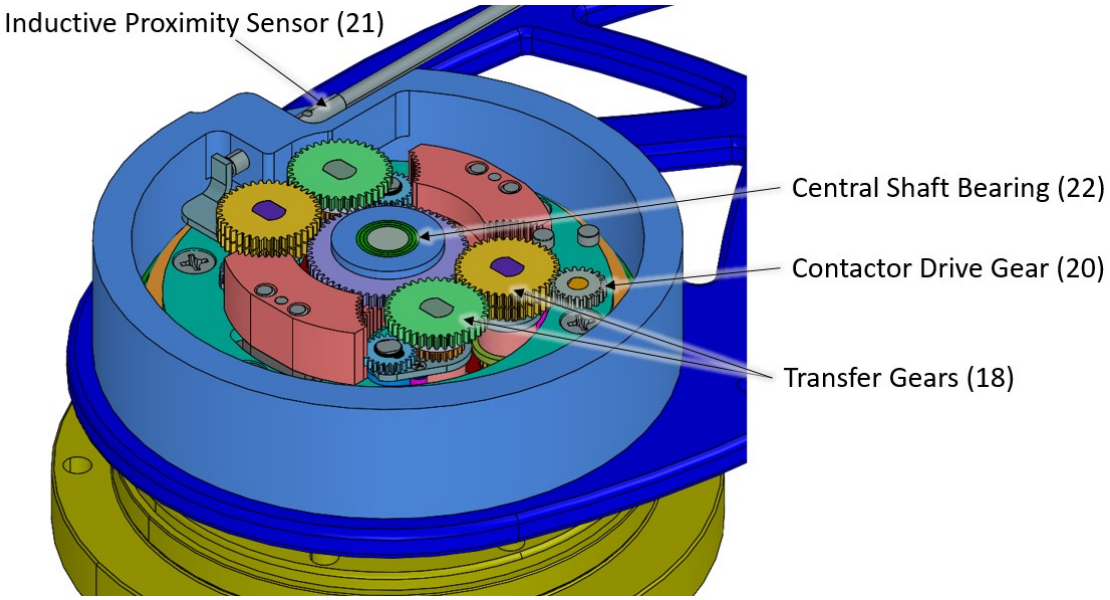

Figure 3.10: VSA drive and transfer gearing giving even symmetry of contactor motion.

Figure 3.11 shows the layer immediately below that shown in Figure 3.10. This layer contains two transfer gears (18) meshed with a central idler gear (5) which provides symmetry of contactor motion to cross-wise pairs of contactors so that all contactors move simultaneously.

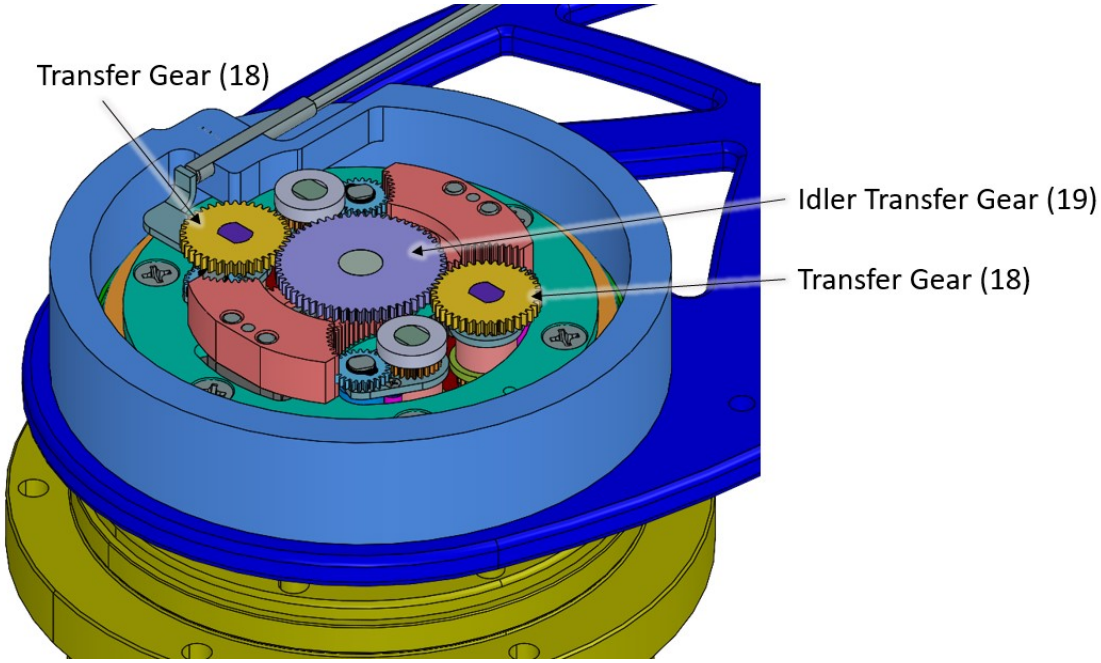

Figure 3.11: VSA transfer gearing giving odd symmetry of contactor motion.

Figure 3.12 highlights the gears that make up the contactor drive system. The contactor motion along the flexure is indicated with a light blue dashed arc. The yellow transfer gears mesh with the green transfer gears on the top layer and with the idler transfer gear on the next layer below. The planetary gearing system consists of a sun, a planet and a ring gear section for each contactor subassembly. The effective gear ratio from the sun gear to the carrier arm contactor motion is 4:1.

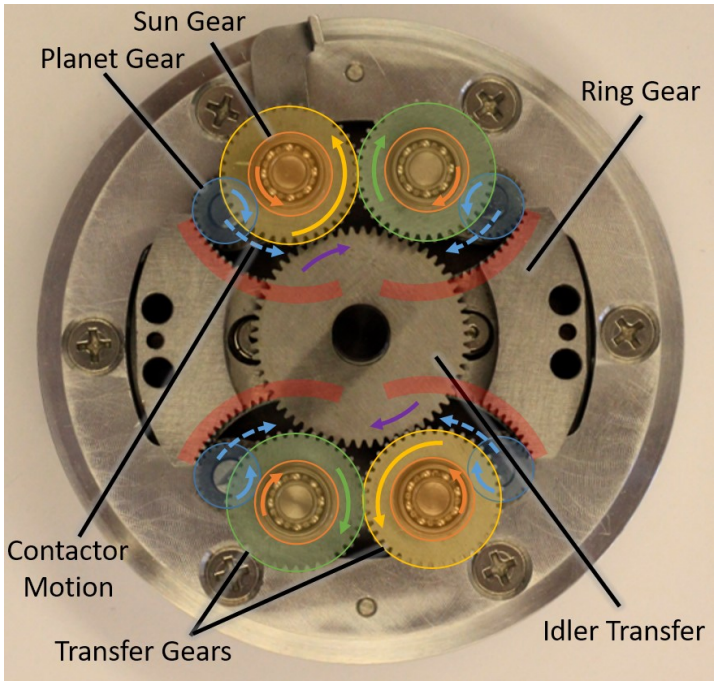

Figure 3.12: Contactor drive gearing system. Transfer gears make all contactors move simultaneously, and planetary gearing increases stiffness of contactor positioning.

3.3 Flexure Stiffness Characteristics

The contactor drive system described above allows joint stiffness to be controlled by driving the stiffness adjustment motor (7), which changes the loading point along the length of the flexure beam. The flexure geometry and material properties determine the relationship between the loading point and the joint stiffness. The maximum deflection at the robot endpoint that can be accommodated without plastic deformation of the flexure determines the minimum stiffness. The maximum stiffness and the nature of the transition between minimum and maximum stiffness are important criteria in the VSA overall performance. A suitable target stiffness range and stiffness change profile are first identified. The use of finite element analysis (FEA) in modeling flexure elastic behavior is described next. Results of tests used to experimentally verify design performance are also presented.

3.3.1 Stiffness Range and Profile

The flexure is designed to provide continuous stiffness variation from very high stiffness to very low stiffness. The goal stiffness variation with respect to contactor position is exponential, which provides constant relative sensitivity. As such, a small deviation or error in contactor position yields a constant proportion variation of the absolute stiffness value. That is, for any operating point *k*, a small angular deviation of the contactor position δφ will create a change in stiffness proportional to operating point stiffness. In equation form,

$$\frac{\delta k}{\delta \varphi} = \lambda k$$

where λ is the constant relating stiffness sensitivity to stiffness. The exponential function satisfying this differential equation is

$$k(\varphi) = k_0 e^{\lambda \varphi};\ \left(0 \leq \varphi \leq \frac{\pi}{2}\right)$$

where φ is the contactor angular displacement from the position of highest stiffness (φ=0) to the position of lowest stiffness (φ=π/2), for which k_0 is the highest stiffness. The stiffness ratio (ratio of maximum stiffness to minimum stiffness) design goal is 1000 or greater. To obtain a stiffness ratio of 1000 for a contactor range of 0 to π/2,

$$\frac{k(0)}{k\left(\frac{\pi}{2}\right)} = 1000$$

$$\frac{k_0}{k_0 e^{\lambda \frac{\pi}{2}}} = e^{-\lambda \frac{\pi}{2}} = 1000$$

$$-\lambda \frac{\pi}{2} = \ln(1000)$$

$$\lambda = -\frac{2}{\pi}\ln(1000) = -4.4$$

Therefore, the desired theoretical relationship between joint stiffness and contactor angle is given by

$$k(\varphi) = k_0 e^{-4.4\varphi};\ \left(0 \leq \varphi \leq \frac{\pi}{2}\right).$$

The magnitude of 4.4 for λ is a design goal minimum. Any magnitude of λ greater than 4.4 will give a stiffness ratio greater than 1000. The flexure geometry consists of tapered curved cantilever beams. The curve on the contactor side of the flexure beam coincides with the arc traced by the contactor tip as it moves through its range of motion. The constant k_0 is affected by the material choice and the beam geometry. The next section describes the procedure used to determine an appropriate shape for the flexure beams used in each joint to achieve the desired stiffness range.

3.3.2 Flexure FEM Analysis and Design

The stiffness of each promising joint flexure design was evaluated using finite element analysis with NX Nastran. To facilitate finite element analysis, the geometry was reduced to a flat surface to use plate type elements. Flexure material and geometry were selected by evaluating different flexure designs with FEA and comparing the stiffness results with the exponential variation desired. Analytical models for straight (non-curved) beam deflection indicated that neither a constant cross section nor a linear taper cross section could be expected to provide an exponential stiffness variation versus contactor position along the length of the beam. A quadratic taper was chosen for the curved flexure beam to achieve a stiffness ratio of at least 1000 between maximum and minimum stiffness with an approximately exponential variation. The side of the beam opposite the contactor was defined by a single arc and ending with a straight section at the beam tip. Three points on the arc defining the beam height at the base, mid-length,

and tip were constrained to give the beam a quadratic taper. By adjusting the beam height at those points and evaluating the corresponding FEA results, a flexure beam geometry that gave the desired stiffness range was identified for each joint.

The analysis for each flexure was run for a large number of contactor positions across its full range. In each load case evaluated, the contactor was given a fixed boundary condition, and a contact model was assigned between the flexure and the contactor. A torque was applied to the outer circumference of the flexure element. The outer circumference was also constrained to only allow rotation about the flexure geometric center, the joint main axis. An example of the resulting deflection and stress from the applied torque on the flexure is shown in Figure 3.13 below. The maximum stress was recorded for each contactor position. The average nodal displacement of the flexure outer circumference was recorded and used to calculate the angular displacement of the loaded flexure.

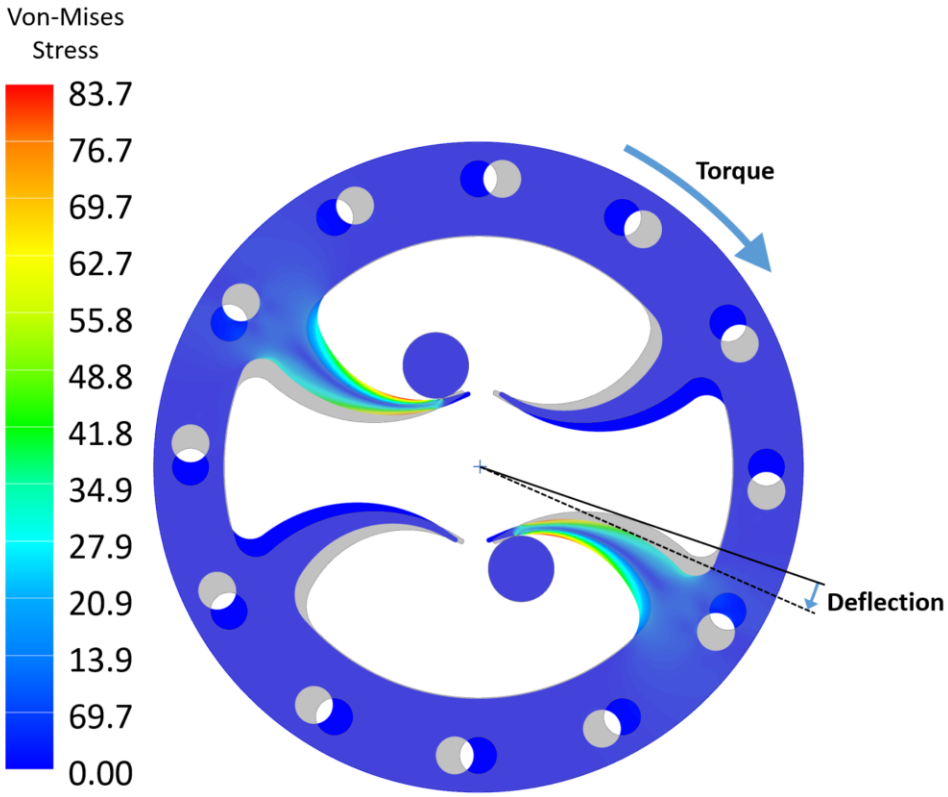

Figure 3.13: Example of FEA stress result for shoulder flexure loaded with a torque on the flexure and fixed contactors. Gray shaded area is the initial (undeflected) position of the flexure.

The minimum stiffness for each flexure was selected so that, when the arm is fully outstretched, at least 13mm of deflection at the manipulator endpoint is accommodated without plastic deformation. As a consequence, flexures closer to the manipulator endpoint have a lower overall stiffness. Two design parameters affecting flexure stiffness and maximum stress are the material and the flexure cross section. For a given amount of deflection, stress (and stiffness) decrease as the flexure cross section height is decreased.

Final selection of material and flexure geometry was based on the desired minimum joint stiffness, a close approximation of the desired exponential stiffness profile, and high maximum stiffness. The shoulder joint selected flexure uses the stiffest

material, titanium, and has the greatest flexure beam cross section. The selected elbow and wrist flexure geometries are thinner in cross section than the shoulder flexure, as shown in Figure 3.14 below. To achieve the desired stiffness range for each, the elbow flexure was made of aluminum, and the wrist flexure of glass-filled nylon.

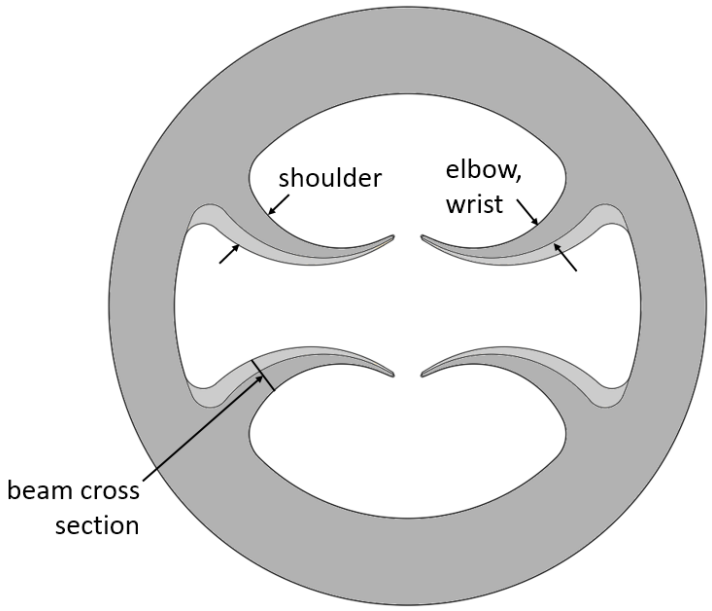

Figure 3.14: Difference in flexure geometry between shoulder and elbow or wrist. The shoulder flexure has a larger beam cross section (beam height) for greater stiffness, but the surfaces that the contactors ride on are the same for all flexures.

The FEA results also defined the allowable torque for the flexures across the range of stiffness settings. At lower stiffness, more deflection can be accommodated but only up to the stress limit of the material.

The numerically obtained stiffness results are summarized in Table 5. The full range of stiffness for each selected flexure is shown in Figure 3.15. The stiffness ratio was over 1000 ($|\lambda|>4.4$) for each flexure, meeting that design goal.

Table 5: Joint Stiffnesses by Numerical Methods

	Material	Joint Maximum Stiffness [Nm/rad]	Joint Minimum Stiffness [Nm/rad]	Stiffness Ratio
Shoulder	Titanium	1.23E+05	34	3610
Elbow	Aluminum	4.92E+04	11.9	4140
Wrist	30% Glass-filled Nylon	5.41E+03	1.83	2960

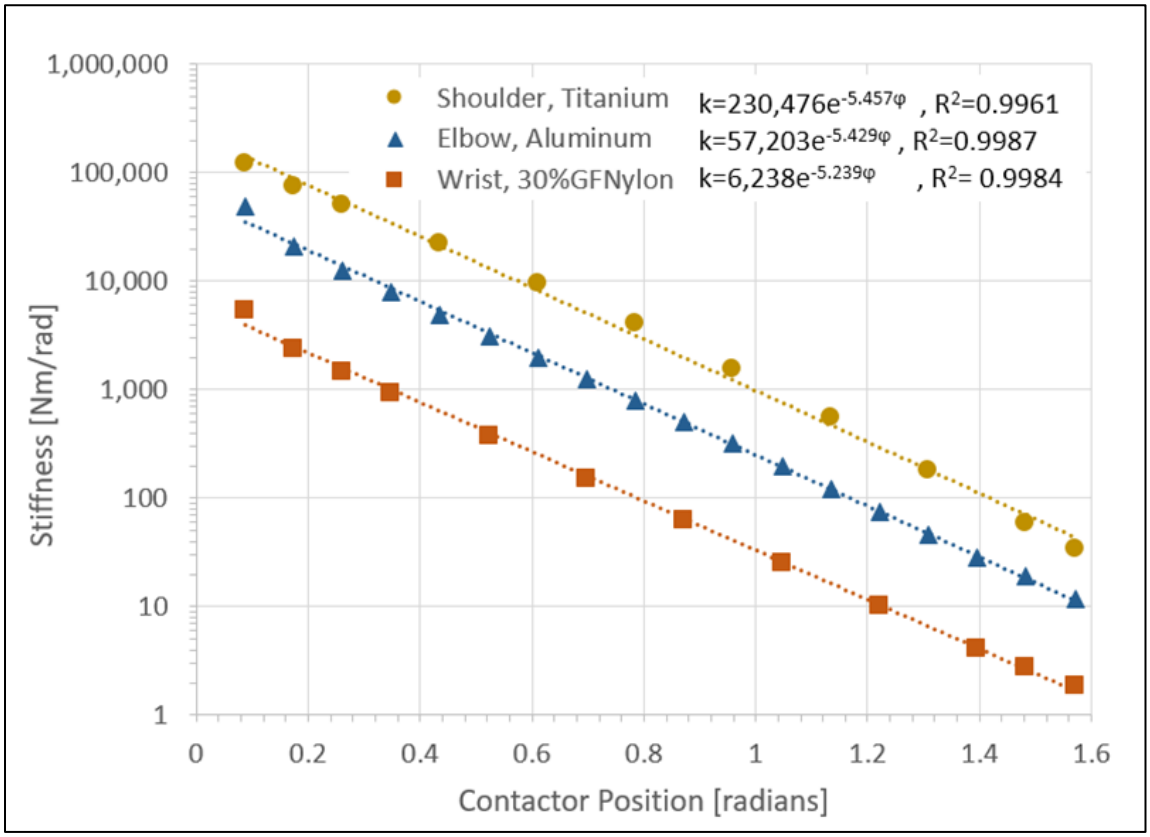

Figure 3.15: Stiffness derived by FEA of shoulder, elbow, and wrist flexures over the range of contactor positions.

3.4 VSA Experimental Performance

The VSA shoulder, elbow, and wrist joints differ only in their three different stiffness ranges. Experimental joint stiffness results were obtained for each VSA by

measuring joint deflection over a range of applied joint torque loads and across the range of contactor positions. A routine programmed in LabVIEW used link weight and angular position to apply a known torque to the joint and automatically collect test data. The joint stiffness testing procedure is described in Appendix B.

The joint stiffness variation time from minimum to maximum stiffness was tested by commanding a trapezoidal velocity motion across the full range. The full stiffness change was achieved in 100 ms.

Figure 3.16 summarizes the experimentally determined relationship between joint stiffness and stiffness actuator position for each of the three joints (shoulder, elbow, and wrist). Joint deflection was recorded for each stiffness actuator position setting as torque on the joint was increased. Stiffness was then computed as the slope of the best-fit line through the collected torque vs. deflection data. A best exponential fit to the data is also illustrated for each joint. These experimentally obtained exponential coefficients are used as system characteristic parameters in the stiffness path planning program.

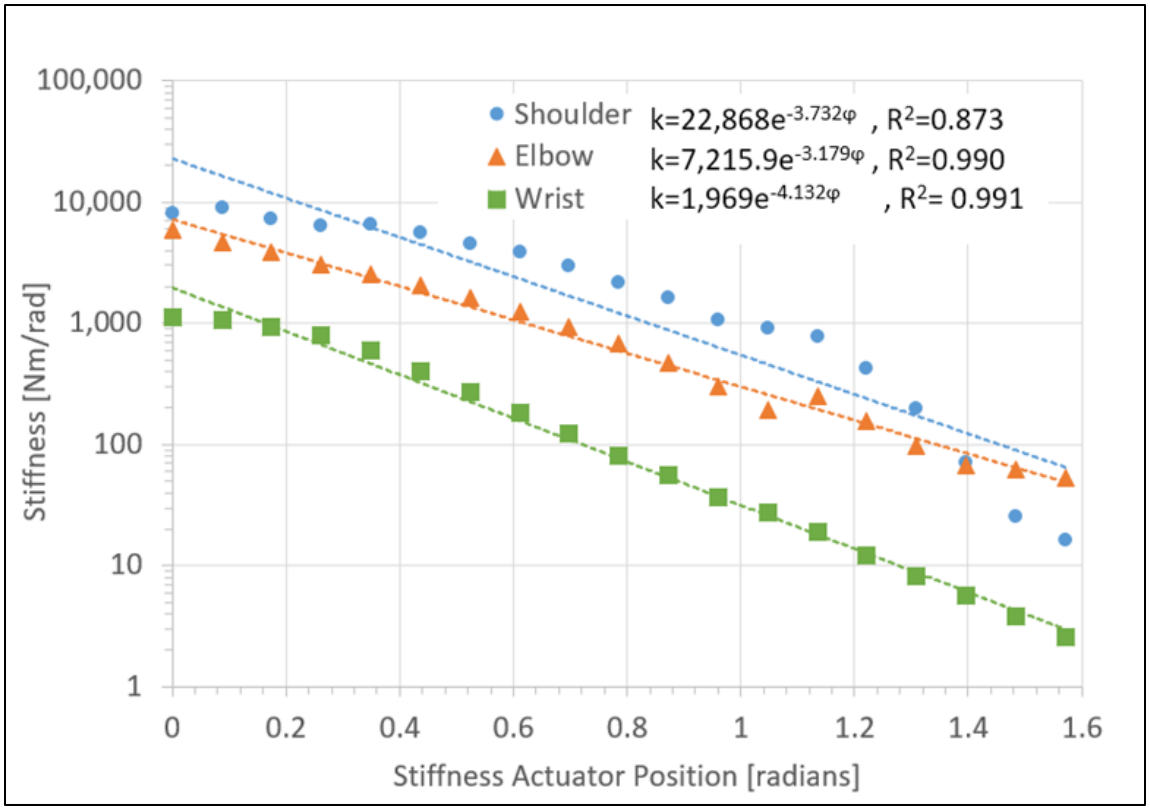

Figure 3.16: Measured stiffness for shoulder, elbow, and wrist joints throughout stiffness range.

The measured stiffness of each joint are summarized below in Table 6. The joint maximum and minimum stiffnesses in the table are those actually measured for each joint rather than the values from the best fit curves. The experimentally measured stiffnesses are used when generating a trajectory for the passive compliance control method [16].

Table 6: Experimentally Measured Joint Stiffnesses

	Joint Maximum Stiffness [Nm/rad]	Joint Minimum Stiffness [Nm/rad]	Stiffness Ratio
Shoulder	8120	16.5	492
Elbow	5830	53.2	110
Wrist	1120	2.61	429

3.5 Discussion

The numerical analysis predicted higher stiffness than what was actually observed experimentally. The simplified model used in the FEA only considered the flexure element, while the measured joint stiffnesses are affected by other components in the VSA as well such as the bearings, contactor shafts, and meshed gears. These other components are expected to have more of an effect on the overall compliance at high stiffness settings, as seen by the lower than expected maximum shoulder stiffness. The lower stiffness elbow and wrist flexures were more likely to be the most compliant element in those joints throughout their stiffness ranges and were closer to the predicted exponential variation. At the lower end of the stiffness ranges, applying a measurement test load torque causes a greater deflection. The deflection changes the loading point of the contactor on the beam and has a stiffening effect which may be responsible for the higher than expected measured stiffnesses at the lower end of the stiffness ranges. Overall, the stiffness ratio as predicted by FEA was more than ten times higher than what was actually achieved. This new VSA design, however, showed an order of magnitude improvement in stiffness ratio compared to the past design using the central shaft flexure.

3.6 Summary

The VSA is a critical component enabling passive compliance control in a robot. In this design, controllable passive compliance is made possible by a novel high-stiffness contactor positioning system and a flexure having a known exponential relationship between contactor position and joint stiffness. The VSA has been designed to give a high maximum stiffness and large stiffness range. Testing indicated that stiffness ratios between 110 and 492 were achieved in the joints, with a variation characteristic close to the desired exponential model. Maximum joint stiffness in the stiffest (shoulder) joint

was 8120 Nm/rad. The experimentally obtained stiffness variation time of 100ms was much better than the design goal of 200ms. The VSA design performance is summarized in comparison to the design goals in Table 7. Compared to the independent stiffness adjustment designs shown in Table 1, the VSA is of comparable stiffness and weight but can actuate through its full range of stiffness faster than any of the other existing designs. The maximum deflection with minimum stiffness for each joint was a design choice based on the joint distance from the robot endpoint and the desire for each joint to be able to accommodate up to a 13 mm deflection at the robot endpoint. The flexure material and geometry for each joint gives the desired maximum deflection without exceeding elastic limits of the flexures. The VSA joints described in this chapter drive the robot arm described in Chapter 2, whose performance is detailed in the following chapter.

Table 7: Achieved VSA Design Parameter Summary

Performance Criterion	Unit	Design Goal	Shoulder	Elbow	Wrist
Full Stiffness Variation Time	[ms]	<200	100	100	100
Maximum torque (at maximum stiffness)	Nm	-	64	28	4.8
Maximum Stiffness	Nm/rad	-	8120	5830	1120
Minimum Stiffness	Nm/rad	-	16.5	53.2	2.61
Stiffness Ratio		>1000	492	110	429
Maximum Deflection with max. Stiffness	Deg	-	0.45	0.28	0.25
Maximum Deflection with min. Stiffness	Deg	-	1.3	2.6	9.1
VSA Mass	kg	<1.0 kg	1.0	1.0	1.0
Weight including Actuator	kg	-	3.5	2.2	1.4

CHAPTER 4

SYSTEM PERFORMANCE VERIFICATION

The robot ability to perform constrained manipulation was tested with a physical task of turning a crank to lift a weight. This is a challenging task to perform with a traditional active force control method since a force sufficient to lift a weight must be applied in the direction that advances the crank, and the direction that force must be applied is continuously changing as the task progresses. At the same time it is desired to minimize forces normal to the direction of crank motion. If a misalignment exists, kinematic constraint forces are generated when interacting with its stiff environment (along crank handle axis). The complete robot system performing the crank-turning task is shown in Figure 4.1 below.

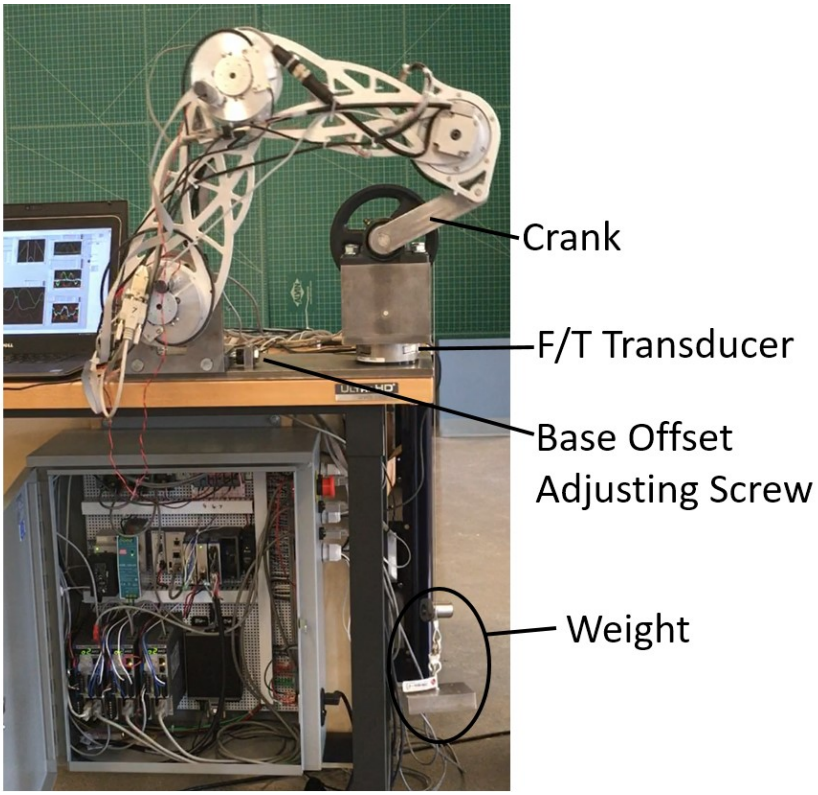

Figure 4.1: Complete robot system performing the crank turning task lifting a weight.

One quantitative measure of robot performance in this manipulation task is the magnitude of kinematic constraint forces experienced during the task execution. Another measure of the robot's performance is the time needed to complete the task, which can depend on the type of control used.

Two modes of operation were compared to assess the performance of the robot. The first mode was passive compliance control, in which positions are commanded and the joint stiffnesses are modulated using variable stiffness actuation. The second mode was active compliance control, where commanded motion proceeded in small steps with position correction performed using measured forces to offset the nominal position commands to reduce kinematic constraint forces. In both modes, the crank angle and forces were measured to compare the resulting constraint forces from the two methods.

4.1 Test Apparatus

The test apparatus consists of the robot and crank mechanisms and the supporting control system components for recording test data. The robot arm and crank are both mounted to a common base plate. Because the robot system and the crank system are each only capable of planar motion, a spherical bearing and sliding shaft are added to the crank handle to accommodate any small discrepancy between the two planes of motion. Angular degrees of freedom are unconstrained by the spherical bearing. The crank geometric parameters are given in Table 8 below. The crank center location is described relative to a coordinate frame located at the center of the robot base joint (as shown in Figure 2.1).

Table 8: Crank Geometric Parameters

Crank center, x	304.8 mm [12 in]
Crank center, y	78.6 mm [3.094 in]
Crank radius	139.7 mm [5.50 in]

The robot base is mounted to a plate which can be moved along the x axis to introduce a position error relative to the nominal crank center location.

The robot control/instrumentation system (updated in Figure 4.2) includes an incremental encoder for measuring the crank angle, and an ATI force/torque transducer 9105-TIF-DELTA to measure forces. The transducer is located under the crank base and sends voltage signals to an analog input module in the c-RIO, sampled every 2 ms. The sensed forces and torques at the crank base are transformed to path tangential and normal forces. The crank encoder was mapped to the HANDWHEEL parameter in one of the servo drives, which the c-RIO also reads at each CANopen cycle every 2 ms.

When using passive compliance control, forces and crank position are only recorded to be able to compare how high the constraint forces are compared to the active compliance control method, but are not used as a control input. When using active compliance control, measured forces are used as a control input for trajectory modification.

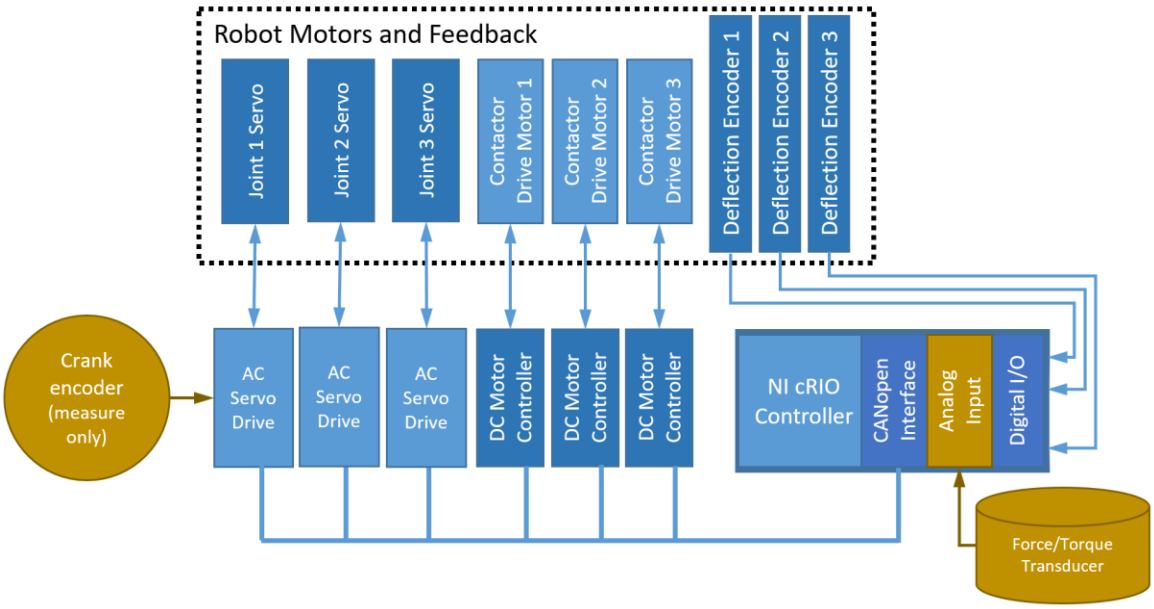

Figure 4.2: Robot control system with crank encoder and force/torque transducer shown.

4.2 Test Procedure

For both the passive and active compliance control methods, before connecting the robot to the crank, the force sensor is first zeroed with the weight suspended from the pulley with the crank rotation locked by a blocking pin inserted through the spokes. The measured forces are then only the robot constraint forces acting on the crank. After zeroing the force sensor, the blocking pin is removed and the robot moved to the starting position of its task trajectory. Once there, the robot is connected to the crank by a rod

fixed to the end of the manipulator and inserted into a spherical bearing in the crank. At this point the robot is supporting the task weight. The weight hanging from the pulley weighs 19.8 N, and the crank pulley radius is 63.5 mm. The crank length is 140 mm. The expected robot applied force to support the hanging weight is

$$\frac{19.8\ \text{N}(63.5\ \text{mm})}{140\ \text{mm}} = 9\ \text{N}.$$

To evaluate the performance of both control methods in the presence of a constraint model error, the robot base location was adjusted to give a 1.6 mm crank center offset in the global x direction, which was enough to show a clear difference between the methods but not so high as to risk damaging the equipment. After zeroing the force sensor, the robot is attached to the crank by positioning the crank to the top center. The robot rotates the crank counterclockwise one full revolution (360 degrees) lifting the weight, then reverses and returns to the starting position, lowering the weight. For the passive compliance control method, the crank was turned using a trapezoidal crank velocity motion profile. For the active compliance control method, a series of 1 mm trapezoidal velocity moves are used to complete the task, discussed further in section 4.4.

4.3 Passive Compliance Control Performance

The passive compliance control method executed a predetermined path in joint position and passive compliance space. Figure 4.3 shows the constrained manipulation task and the test apparatus. The compliance ellipse changes orientation throughout the task to maintain a greater compliance in the direction normal to the path, and a relatively small compliance in the direction tangential to the path to ensure progress is made in advancing the crank. The force/torque transducer measures forces acting on the crank during the task execution. The measurements are zeroed before starting the task with the

weight already hanging from the pulley so that any recorded forces are due only to the robot interacting with the crank.

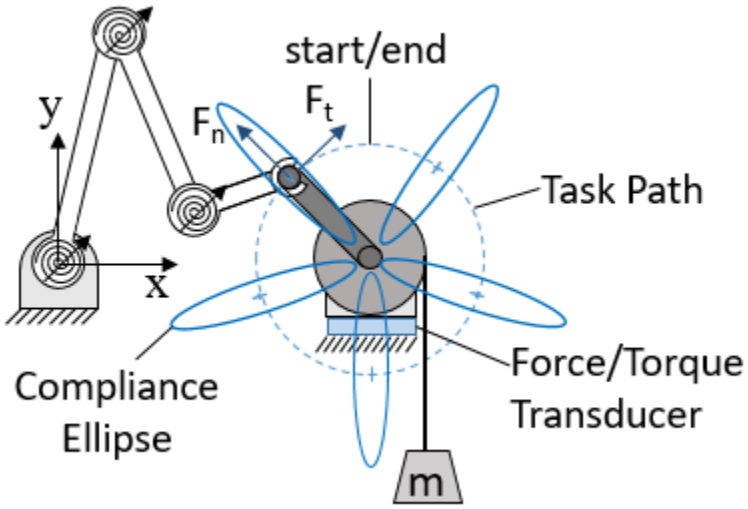

Figure 4.3: Constrained manipulation test apparatus showing crank turning to lift a weight. Force/Torque transducer records constraint forces. Path is followed by open loop position and passive compliance control.

The joint position and stiffness actuator trajectories followed by the robot using the passive compliance control are shown in Figure 4.4 and Figure 4.5. The methodology of generating these trajectories through task and compliance space is covered in [16], and require a priori models (ideally experimentally obtained) of the robot links and joint stiffness variation characteristics. The trajectories shown give a compliance ratio of 6 throughout the task execution and lift the weight in 6.1 seconds.

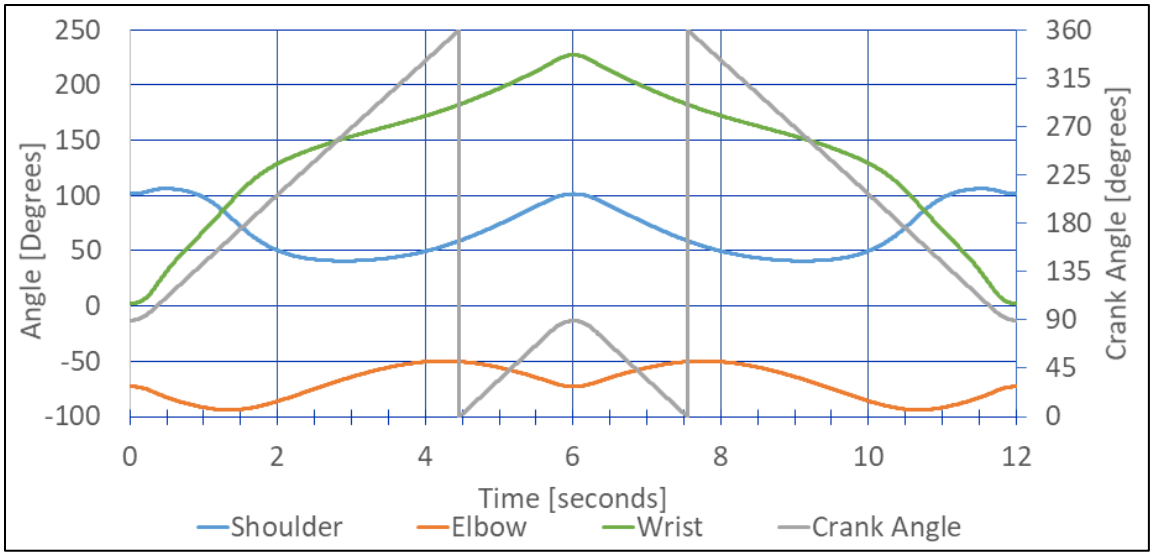

Figure 4.4: Joint position trajectories to turn the crank one full revolution lifting the weight and one full revolution lowering the weight back to starting position using passive compliance control.

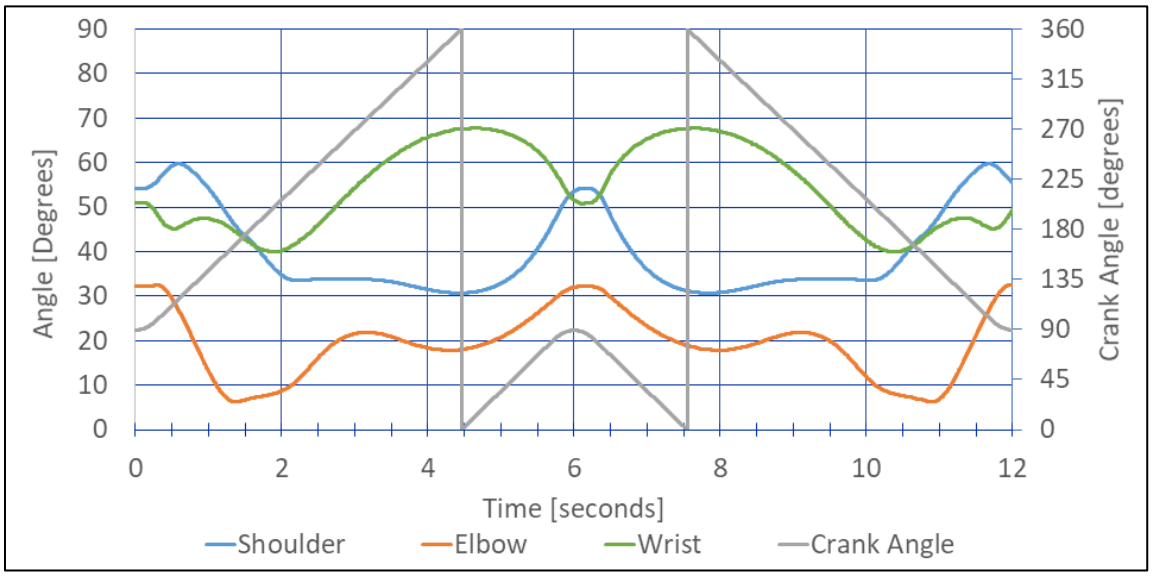

Figure 4.5: Stiffness actuator trajectories to turn the crank one full revolution lifting the weight and one full revolution lowering the weight back to starting position using passive compliance control. Stiffness actuator trajectories control the compliance of each joint and together with the joint positions, the robot endpoint compliance.

The constraint forces acting on the crank during the task using the passive compliance control are shown in Figure 4.6. Forces were sampled every 2ms during the 6.1 seconds it took to make one revolution of the crank. The forces are presented in path

tangential and path normal components over the span of one full crank cycle of one revolution first raising and then lowering the weight. The path tangential force averages approximately 10 N which balances the weight suspended by the pulley. The path normal force has a peak to peak variation of approximately 15 N.

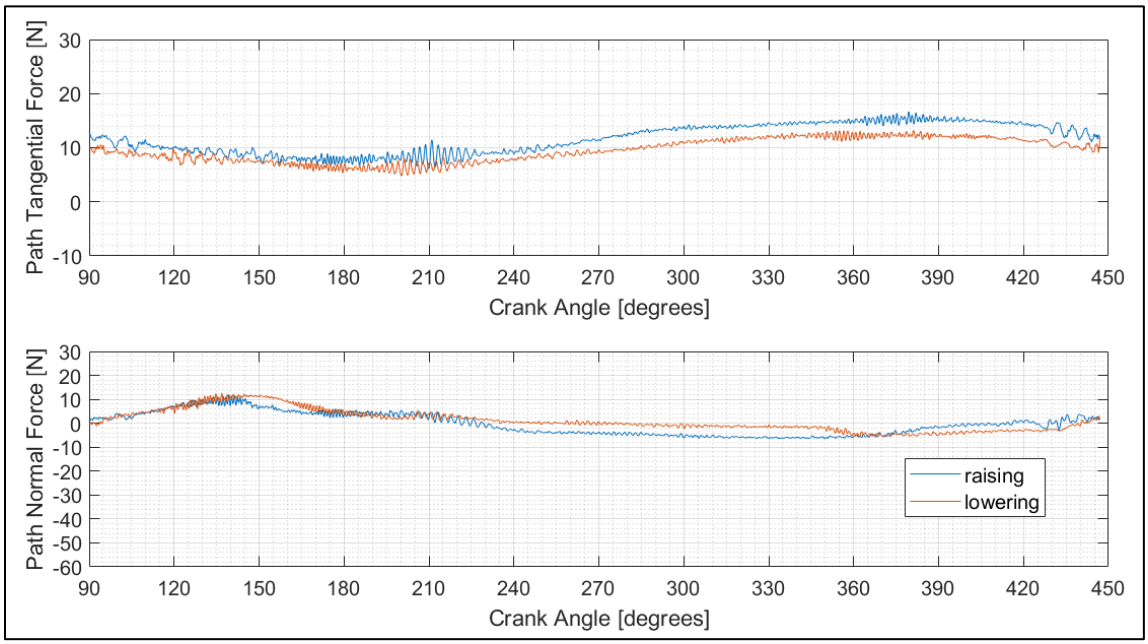

Figure 4.6: Path tangential and normal forces for passive compliance control method.

4.4 Active Compliance Control Performance

In the active compliance control approach, a correction is applied to the position commands based on the measured forces. The control law is

$$\boldsymbol{x} = \boldsymbol{x}_0 + \boldsymbol{x}_c = \boldsymbol{x}_0 + \boldsymbol{C}\boldsymbol{f}$$

where $\boldsymbol{x}$ is the actual commanded position, $\boldsymbol{x}_0$ is the nominal commanded position, and $\boldsymbol{x}_c$ is the corrective motion determined by forces $\boldsymbol{f}$ acting on the end-effector. For the planar task, the active compliance matrix described in the global xy coordinate frame defined in Figure 4.3 is

$$\boldsymbol{C} = \begin{bmatrix} c_{\mathrm{x}} & c_{\mathrm{xy}} \\ c_{\mathrm{yx}} & c_{\mathrm{y}} \end{bmatrix} = \begin{bmatrix} 3 \times 10^{-5} & 0 \\ 0 & 3 \times 10^{-5} \end{bmatrix} \mathrm{m/N}$$

Using the active compliance approach, a motion setpoint is reached, forces are measured, and the forces are multiplied by the fixed compliance matrix $\boldsymbol{C}$ to give an offset for the next motion command. Figure 4.7a illustrates different sequences of motions. The dashed line is the nominal path that would be commanded and followed in the absence of any constraint forces. The solid line is the real path providing constraint to the robot. The difference between the two results in a constraint force acting on the robot. With active compliance control, the modification of each next motion setpoint is proportional to the sensed force. The proportional constant (diagonal matrix $\boldsymbol{C}$) is the active compliance control feedback gain. The solid dots are commanded positions, $\boldsymbol{x}$. The empty dots are the nominal path points $\boldsymbol{x}_0$.

Figure 4.7a-d show the importance of selecting an appropriate value for the active compliance $\boldsymbol{C}$ relative to $\boldsymbol{C}_{\mathrm{sys}}$, the system passive compliance. $\boldsymbol{C}_{\mathrm{sys}}$ is the total real compliance from both the robot itself and the environment with which it is interacting. The active compliance is desired to be large to reduce constraint forces, but instability can occur when the active compliance is greater than the passive system compliance as observed in Figure 4.7d. The practical implication for traditionally stiff (low $\boldsymbol{C}_{\mathrm{sys}}$) robots performing a constrained manipulation task is that one cannot just expect to keep lowering constraint forces by increasing active compliance $\boldsymbol{C}$ without limit. Stable operation requires careful tuning of the active compliance which can be time-consuming to set up and risky to implement if appropriate machine safeguards are not in place. The value of $3\text{x}10^{-5}$m/N used here was as high as could be practically used before instability started becoming a problem.

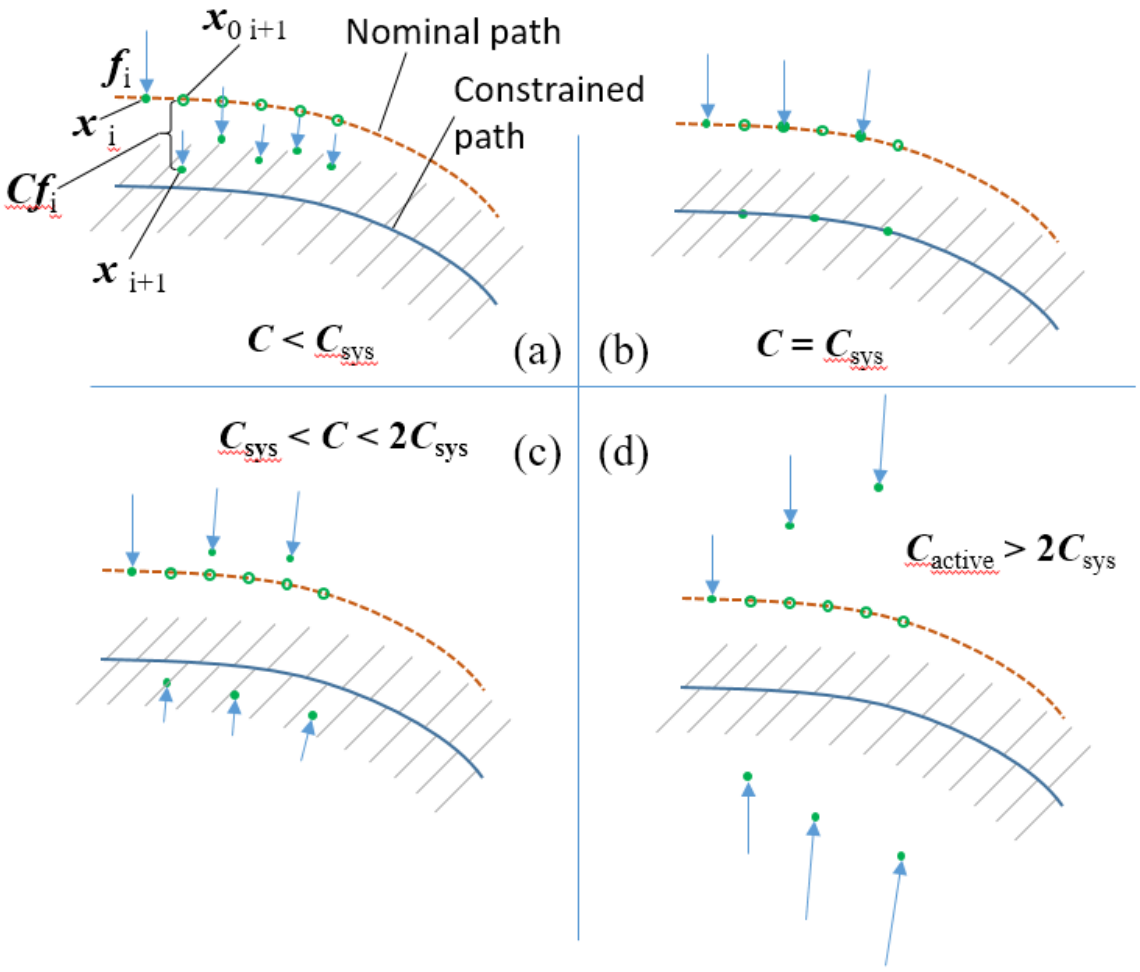

Figure 4.7: Illustration of effect of active compliance ***C*** *relative to system passive compliance* ***Csys*** *when using active compliance control. Case (a) is desired behavior while others will show instability.*

When evaluating the active compliance control approach, the VSA joints are set to their maximum stiffness so the robot behaves as a stiff manipulator capable of accurately following the position commands. The nominal path is computed using inverse kinematics, with the wrist joint oriented to always pull the crank. The signs of the measured forces (those acting on the crank) are reversed to obtain the forces acting on the manipulator. The forces acting on the manipulator are then multiplied by the compliance matrix (motor feedback gains).

The robot crank turning path is divided into a series of points 1mm apart circumferentially. A trapezoidal velocity profile was used for motion in each 1mm step, with 100 ms to complete the motion followed by a pause for 100 ms to measure the forces, as illustrated in Figure 4.8.

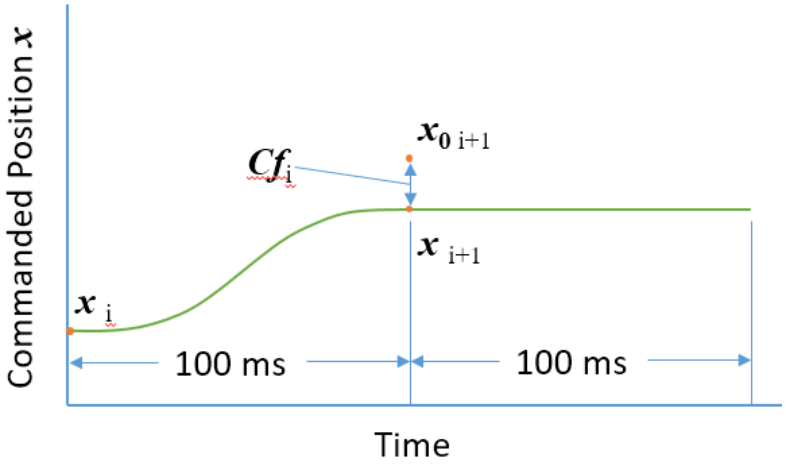

Figure 4.8: Active stiffness control theoretical motion profile. Robot pauses 100ms after each move to measure forces and calculate a position offset.

The commanded motion induces vibration in the system with a ringing frequency of approximately 36 Hz as shown in Figure 4.9. The sampling rate of the force data is 2 ms, but to get a reliable measurement, samples are averaged over 4 periods of the vibration ringing which corresponds to the 100ms force measurement time. The many short moves with the requirement of starting from and coming to a complete stop to measure forces before making the next move results in a significantly longer time to complete the task. The time to make one full revolution with the crank (raising or lowering) was 175.4 seconds using the active compliance control approach.

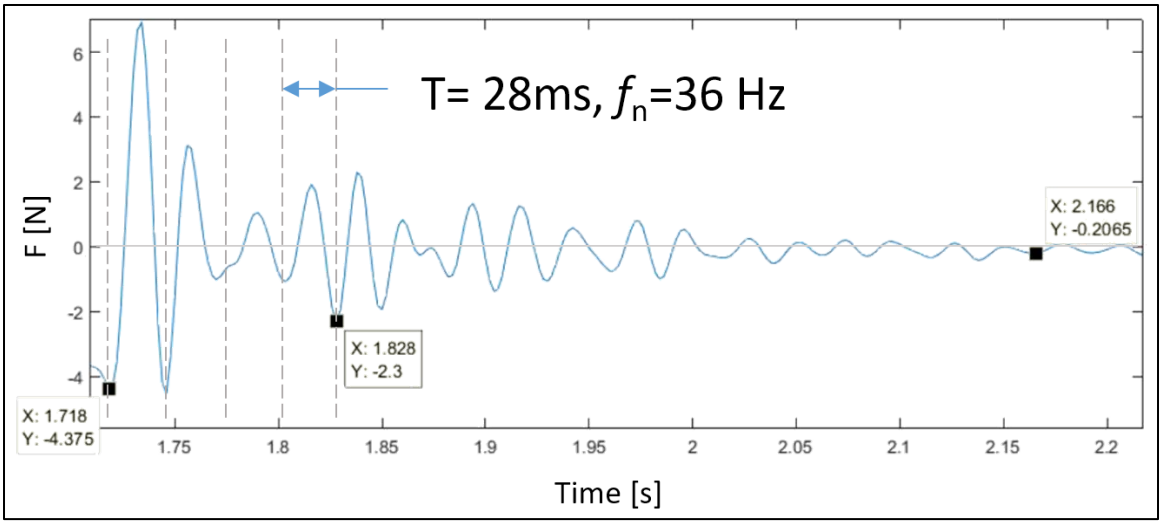

Figure 4.9: Force measurement of the robot system following a step motion input. Ringing at 36 Hz is observed.

The 3R manipulator is kinematically redundant for particle planar motion. To eliminate the redundancy, the wrist link was constrained to have a constant angular position relative to the crank angle throughout the task as stated previously. The joint trajectories could then be determined by inverse kinematics. The joint trajectories used for the active compliance control method are shown in Figure 4.10. A portion of the same data is shown in Figure 4.11 which shows the intervals of motion and stopping for force measurement. At such small increments of motion the discretization of the crank angle encoder is also evident, which is noted in Figure 4.11.

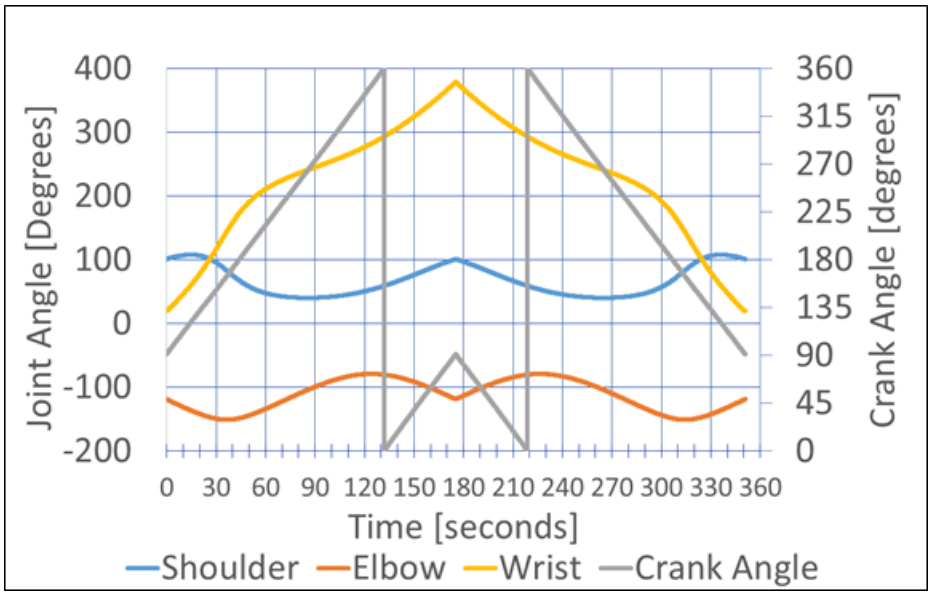

Figure 4.10: Force feedback commanded joint trajectories for turning the crank one full revolution and returning to start position.

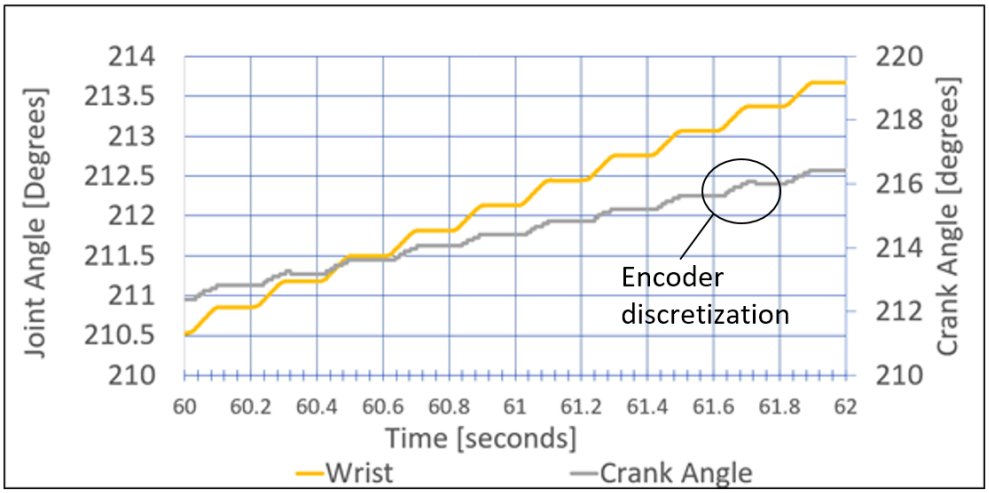

Figure 4.11: Zoomed in view of trajectories for active compliance control method showing motion and hold (measurement) intervals.

The forces recorded for turning the crank using the active compliance control method are shown in Figure 4.12. The forces shown are the unfiltered data obtained by the force sensor every 2 ms for directions tangential and normal to the path. The average tangential force is similar to that seen in the passive compliance control. The path normal forces are much higher, with a peak to peak variation of approximately 80 N.

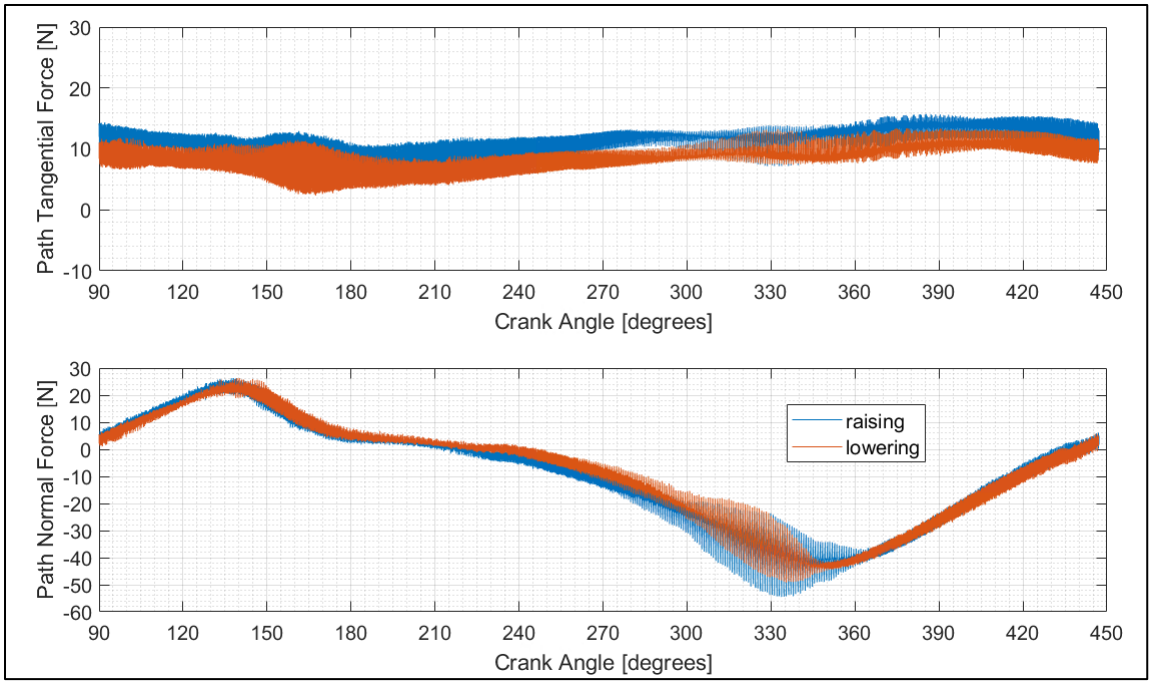

Figure 4.12: Path tangential and normal forces for active force control method.

4.5 Discussion and Summary of Results

The two performance metrics of interest to compare the passive and active compliance control methods are the time to turn the crank and the constraint forces at the robot end effector.

Regions of instability were observed in the constraint force results for the active control mode and can be explained by the configuration-dependent passive compliance of the robot being relatively low in those portions of the task. Possible improvements to the VSA performance and overall reliability are discussed in this chapter. Other areas of potential further research with the robot system are also identified to make use of the controllable passive compliance.

4.6 Time to Turn Crank

The time to turn the crank one full revolution with each control method is listed in Table 9. At 6.1 seconds, the passive compliance control method is 29 times faster than

the active compliance control method. At faster speeds, dynamic effects in the passive compliance control method triggered the flexure overload protection response. For the active compliance control approach, speed is limited by the time required to measure forces after each incremental move. Larger incremental moves would reduce task time but would also result in even larger forces. More frequent moves would require using unreliable contact force information.

Table 9: Time to complete the one full crank rotation

	Task Completion Time
Open-loop VSA Position/Compliance Control	6.1s
Closed Loop Force Feedback Control	175.4s

4.7 Constraint Forces

The constraint forces for each control method are shown in Figure 4.6 and Figure 4.12. Path tangential forces are similar in the two methods and equivalent to the 9N force required to lift the weight calculated in Section 4.2. The path normal forces for the active compliance control method are about five times greater than those using the passive compliance control.

To better understand the high amplitude force oscillation observed in portions of the path when using active compliance control, the passive compliance of the robot when each joint stiffness is at its highest value is investigated. The Cartesian passive compliance of the robot end effector is shown in Figure 4.13 for the active compliance control method. Even though the joint passive compliances were held fixed at their stiffest settings, the end effector Cartesian compliance is a function of robot configuration, which changes throughout the task. The Cartesian compliance values in Figure 4.13 are calculated using Eqn. (1) and joint compliances corresponding to the

maximum joint stiffnesses listed in Table 6. The compliance of the robot link structures are not included because they are negligible relative to the joint compliances. Note that the robot Cartesian passive compliance is a similar order of magnitude as the compliance chosen as feedback gains of $3x10^{-5}$ m/N.

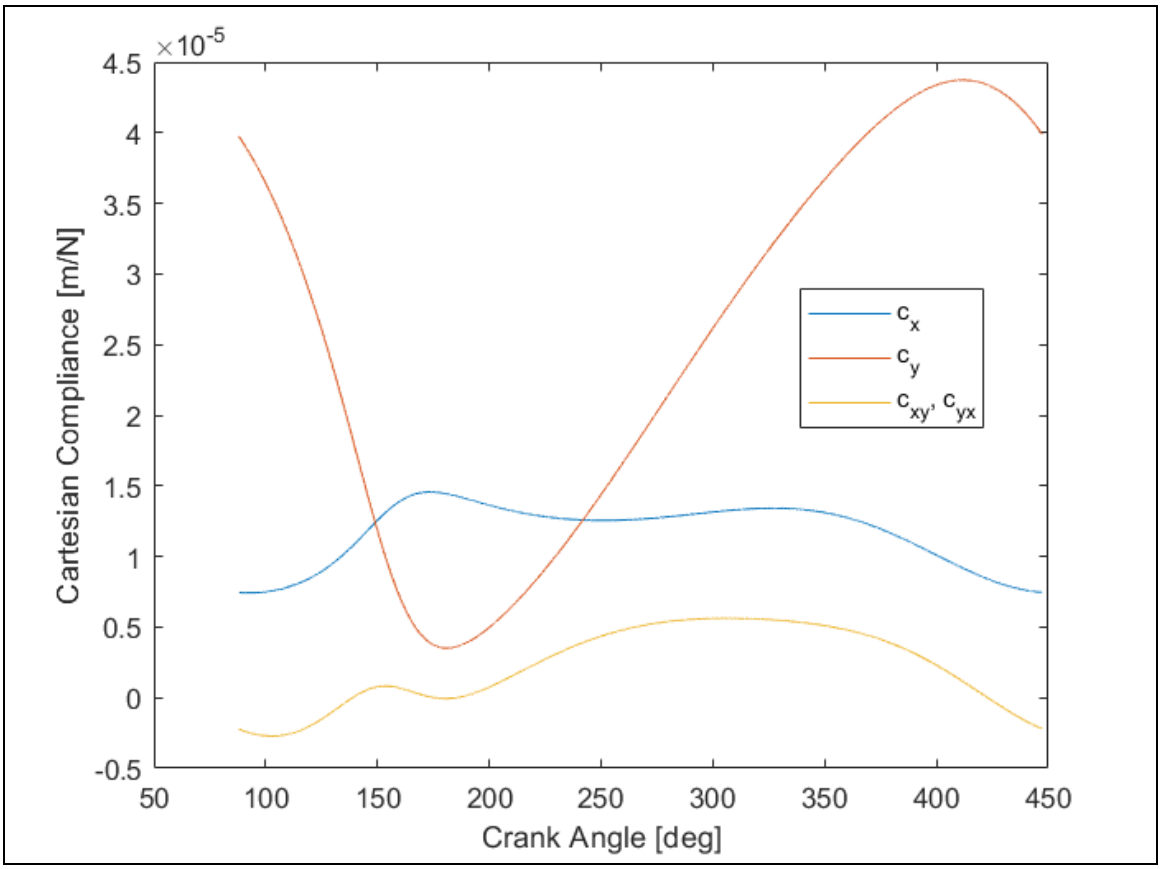

Figure 4.13: Configuration-dependent Cartesian passive compliance of robot end effector for force control method.

There are two regions where instability is observed in the force measurements using active compliance control (see Figure 4.12). These are observed: 1) in the path tangential force when the crank angle is between approximately 150 and 180 degrees, and 2) in the path normal force when the crank angle is between approximately 300 and 360 degrees. These configurations are shown in Figure 4.14.

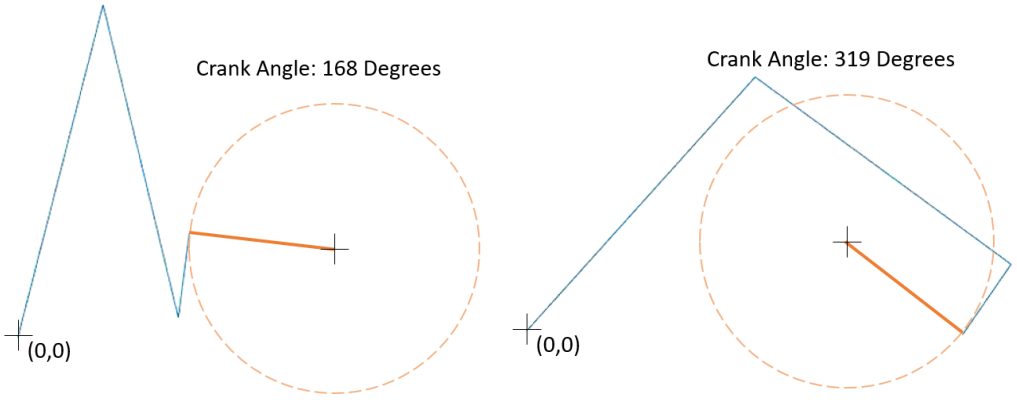

Figure 4.14: Robot configurations in regions of observed force instability.

At a crank angle of 168 degrees, the path tangential force is close to the global y direction. In this configuration, the c_y compliance element is aligned with the global y direction and is at a minimum near the same crank angle (see Figure 4.13.) When the active compliance is more than twice the passive compliance, an overcorrection occurs which generates an even larger force than the one initially being compensated for, leading to a condition of instability. At a crank angle of 319 degrees, the instability may be caused by the crank supporting more of the weight of the robot as it is outstretched further, as no gravity compensation was used for the active compliance control method.

Figure 4.15 is a rotated version of the global Cartesian compliance matrix elements of Figure 4.13. Matrix transformations are applied to obtain the passive compliance of the robot in the path normal (n) and tangential (t) components throughout the task. It shows that the passive normal component is less than ½ the active compliance of 3×10^{-5} m/N in the regions of observed instability (areas below the dashed line at 1.5×10^{-5} m/N). Any increase in the active compliance in an attempt to reduce interaction forces would instead result in even greater instability and larger forces.

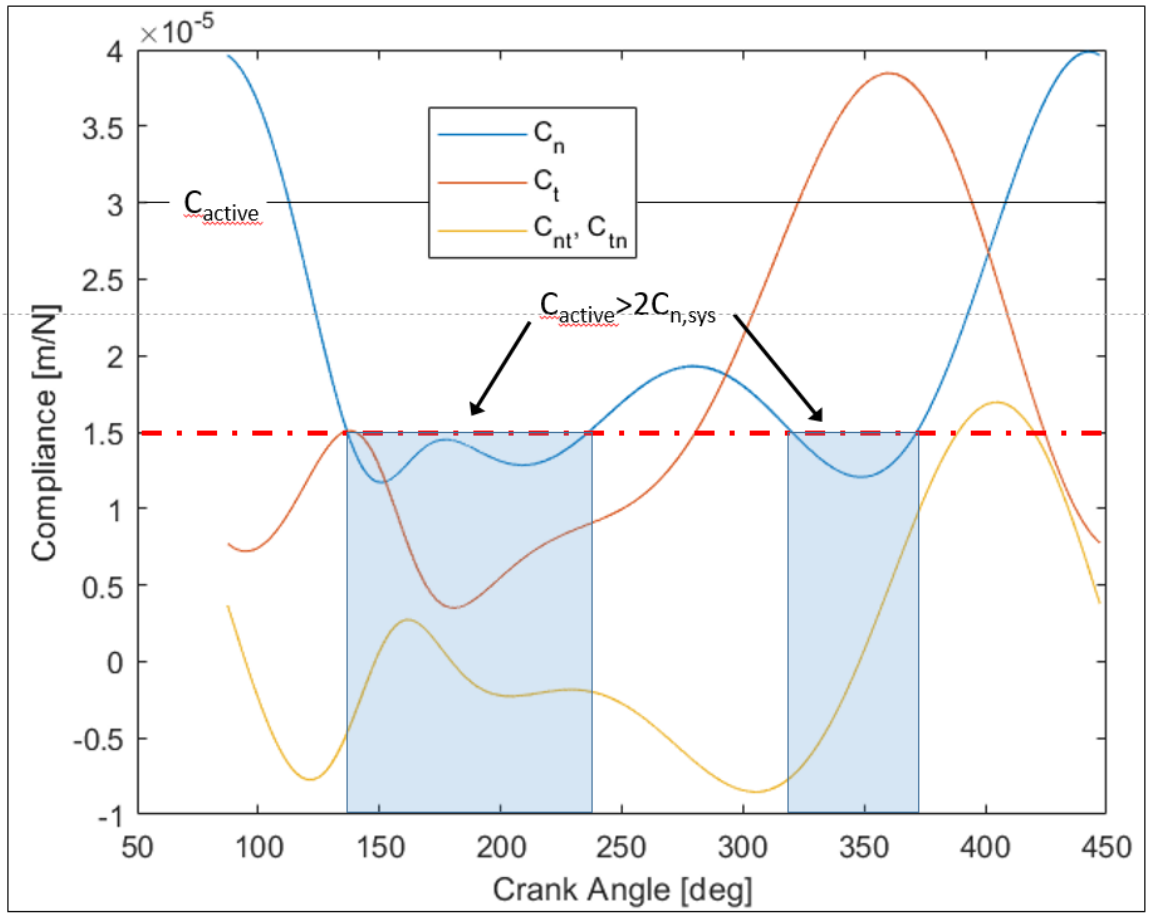

Figure 4.15: Robot end effector compliance in path normal and tangential coordinate system.

CHAPTER 5

CONCLUSION

The VSA joints successfully varied the passive compliance of the robot arm, making the passive compliance control possible and validating the trajectory planning method detailed in [16]. The VSA joints achieved an exponential stiffness variation with stiffness ratios between 110 and 492, an order of magnitude more than the previous arched flexure design [14]. The VSA could actuate through the full stiffness range in 100 ms making it the fastest among existing independent stiffness adjustment designs identified in Table 1. The robot successfully implemented the passive compliance control method to complete the bilaterally constrained manipulation task of turning a crank, demonstrating a real application of VSA joints in a multi-DOF robot which has not been shown before in the literature. The passive compliance control method greatly outperformed the more traditional active compliance control method in both increased speed and reduced magnitude of constraint forces. The passive compliance control method was nearly thirty times faster and experienced forces less than one fifth of those seen in the active compliance control method.

5.1 Possible Design Refinements

The robot successfully demonstrated the strength of passive compliance control relative to active compliance control, and even greater performance could be achieved with a number of improvements that could be made to the system. The usable task space of the robot for a full range of stiffness values is limited by the torque ratings of the flexures which decrease as the stiffness setting is reduced. Increased load capacity could

be achieved by increasing the number of flexure elements and reducing their beam cross sections to reduce the stress for a given deflection. The load carrying capacity of the robot arm as a whole could also be improved by reducing the weight of the VSA. While the planetary gearing inside the VSA was intended to increase stiffness, it is possible that the complexity of the mechanism still introduced some unwanted compliance and unnecessary weight. Additionally, while the system was designed to be planar, future similar designs would be well advised to include out-of-plane stiffening elements to mitigate any unintended out-of-plane compliance. Advances in 3D printing could make new designs possible incorporating composite materials and spatially varying lattice geometries for custom tuning of compliant elements.

The flexures have deflection limits which must not be exceeded to ensure they do not plastically deform. The current design monitors the deflection electronically and stops motion if a limit is reached. Mechanical hard stops inside the VSA protecting the flexure would provide additional safety and improve robustness of the robot.

5.2 Passive Compliance Control Development

Robot dexterity could be dramatically improved using the passive compliance control approach in many more applications. The testing done here assumed a quasistatic operation, i.e., forces due to system dynamics were not taken into account. At faster speeds, these forces can become significant. These forces can also be a desirable feature when a task involves fast motion or impact loads, such as in throwing an object or hammering a nail. High compliance along the direction of impact would isolate the robot from large forces that would otherwise cause damage with a very stiff manipulator. The novel implementation of passive compliance control on a first of its kind 3DOF VSA

driven robot arm opens possibilities for more new applications requiring time and space varying compliance in constrained manipulation tasks.

BIBLIOGRAPHY

[1] S. Huang and J. M. Schimmels, "Realization of point planar elastic behaviors using revolute joint serial mechanisms having specified link lengths," *Mechanism and Machine Theory,* vol. 103, pp. 1-20, 2016.

[2] S. Wolf, G. Grioli, O. Eiberger, W. Friedl, M. Grebenstein, H. Höeppner, E. Burdet, D. G. Caldwell, R. Carloni, M. G. Catalano, D. Lefeber, S. Stramigioli, N. Tsagarakis, M. Van Damme, R. Van Ham, B. Vanderborght, L. C. Visser, A. Bicchi and A. Albu-Schäffer, "Variable Stiffness Actuators: Review on Design and Components," *IEEE/ASME Transactions on Mechatronics,* vol. 21, no. 5, pp. 2418-2430, 2016.

[3] B.-S. Kim and J.-B. Song, "Hybrid Dual Actuator Unit: A Design of a Variable Stiffness Actuator Based on an Adjustable Moment Arm Mechanism," in *IEEE International Conference on Robotics and Automation*, Anchorage, AK, USA, 2010.

[4] M. Garabini, A. Passaglia, F. Belo, P. Salaris and A. Bicchi, "Optimality Principles in Variable Stiffness Control: The VSA Hammer," in *IEEE/RSJ International Conference on Intelligent Robots and Systems*, San Francisco, CA, USA, 2011.

[5] M. G. Catalano, G. Grioli, M. Garabini, F. Bonomo, M. Mancini, N. Tsagarakis and A. Bicchi, "VSA-CubeBot: A Modular Variable Stiffness Platform for Multiple Degrees of Freedom Robots," in *IEEE International Conference on Robotics and Automation*, Shanghai, China, 2011.

[6] F. Petit, M. Chalon, W. Friedl, M. Grebenstein, A. Albu-Schäffer and G. Hirzinger, "Bidirectional Antagonistic Variable Stiffness Actuation: Analysis, Design & Implementation," in *IEEE International Conference on Robotics and Automation*, Anchorage, Alaska, USA, 2010.

[7] W. Friedl, M. Chalon, J. Reinecke and M. Grebenstein, "FAS A Flexible Antagonistic Spring Element for a High Performance Over," in *IEEE/RSJ International Conference on Intelligent Robots and Systems*, San Francisco, CA, USA, 2011.

[8] M. G. Catalano, G. Grioli, F. Bonomo, R. Schiavi and A. Bicchi, "VSA-HD: From the Enumeration Analysis to the Prototypcial Implementation," in *IEEE/RSJ International Conference on Intelligent Robots and Systems*, Taipei, Taiwan, 2010.

[9] A. Jafari, N. G. Tsagarakis and D. G. Caldwell, "AwAS-II: A New Actuator with Adjustable Stiffness Based on the Novel Principle of Adaptable Pivot Point and Variable Lever Ratio," in *IEEE International Conference on Robotics and Automation*, Shanghai, China, 2011.

[10] S. Wolf, O. Eiberger and G. Hirzinger, "The DLR FSJ: Energy Based Design of a Variable Stiffness Joint," in *IEEE International Conference on Robotics and Automation*, Shanghai, China, 2011.

[11] M. Mancini, G. Grioli, M. G. Catalano, M. Garabini, F. Bonomo and A. Bicchi, "Passive Impedance Control of a Multi-DOF VSA-CubeBot Manipulator," in *International Conference on Robotics and Automation*, 2012.

[12] L. Balletti, A. Rocchi, F. Belo, M. Catalano, M. Garabini, G. Grioli and A. Bicchi, "Towards Variable Impedance Assembly: the VSA Peg-In-Hole," in *International Conference on Humanoid Robots*, 2012.

[13] B.-S. Kim, Y.-L. Kim and J.-B. Song, "Preliminary Experiments on Robotic Assembly Using a Hybrid-Type Variable Stiffness Actuator," in *International Conference on Advanced Intelligent Mechatronics*, 2011.

[14] D. Garces, "Design and Verification of a Compact Variable Stiffness Actuator With a Very Large Range of Stiffness," Marquette University, 2014.

[15] J. J. Rice and J. M. Schimmels, "Passive Compliance Control of Redundant Serial Manipulators," *J. Mechanisms Robotics,* vol. 10, 2018.

[16] J. J. Rice, "Passive Compliance Control of Redundant Serial Manipulators," Marquette University, 2019.

[17] S. S. Groothuis, G. Rusticelli, A. Zucchelli, S. Stramigioli and R. Carloni, "The Variable Stiffness Actuator vsaUT-II: Mechanical Design, Modeling, and Identification," *IEEE/ASME Transactions on Mechatronics,* vol. 19, no. 2, pp. 589-597, 2014.

[18] W. Wang, Y. Zhao and Y. Li, "Design and Dynamic Modeling of Variable Stiffness Joint Actuator Based on Archimedes Spiral," *IEEE Access,* vol. 6, pp. 43798-43807, 2018.

[19] W. Wang, X. Fu, Y. Li and C. Yun, "Design of Variable Stiffness Actuator Based on Modified Gear-Rack Mechanism," *ASME Journal of Mechanisms and Robotics,* vol. 8, p. 061008, 2016.

[20] O. Eiberger, S. Haddadin, M. Weis, A. Albu-Schäffer and G. Hirzinger, "On Joint Design with Intrinsic Variable Compliance: Derivation of the DLR QA-Joint," in *IEEE International Conference on Robotics and Automation*, Anchorage, AK, USA, 2010.

[21] E. Sariyildiz, R. Mutlu, J. Roberts, C.-H. Kuo and B. Ugurlu, "Design and Control of a Novel Variable Stiffness Series Elastic Actuator," *IEEE/ASME Transactions on Mechatronics,* vol. 28, no. 3, pp. 1534-1545, 2023.

Appendix A ROBOT SUPPORTING FUNCTIONALITIES

Besides the novel variable stiffness functionality implemented in the robot, other supporting and safety features add to the robustness and utility of the robot as a system, including joint homing and deflection monitoring. The joint homing functionality is described below.

A.1 Inductive Proximity Sensors for Homing

The robot joint positions are measured with incremental rather than absolute encoders, so joint homing must be performed every time the robot is powered on. Each joint has an inductive proximity sensor which senses a target mounted on the subsequent link. The homing target must be moved to the appropriate side of the homing sensor before the homing routine is begun. Every joint begins homing with a counterclockwise motion. The homing routine moves the selected joint until the homing sensor detects the first edge of the homing target. The joint continues to move 10 degrees past that first edge so it is no longer sensing the homing target. The last step in the routine is a reverse (CW) joint homing motion to sense the other edge of the homing target. The center of the homing target is thus calculated to be located at the average encoder count of the two edges, and an offset is applied to make the new zero position correspond to a horizontal link orientation in the case of the first link, and a zero relative angle between subsequent links. A LabVIEW VI performs all of the homing routine steps in sequence automatically for the selected joint and puts the corresponding servo drive in manual motion mode when finished homing.

Contactor angles are also homed by an inductive proximity sensor installed in each VSA. The homing routine runs the contactor motor in the direction that stiffens the

joint until the sensor detects the homing target which extends from one of the contactor carrier arms. The home zero position for the contactors corresponds to the maximum stiffness setting.

A.2 Deflection Monitoring

The flexures are designed to flex without permanent plastic deformation. There is a tradeoff between compliance and load bearing capacity of each flexure. As the loading point of the flexure moves towards the tip of the flexure beam, deflection increases but so do stresses for a given load. The allowable torque limit for each flexure is dependent on the flexure material, shape, and stiffness setting (location of contactor along the flexure). The robot control program includes a monitoring function which compares the deflection of each flexure during every control cycle with the theoretically determined allowable deflection given the current stiffness setting of each joint. If an overload condition is sensed for three consecutive control cycles (comprising 6 milliseconds), a fault is generated and motion is stopped.

Appendix B JOINT STIFFNESS MEASUREMENT

The sequence of operations of the joint stiffness testing routine is shown in Figure B.1 below.

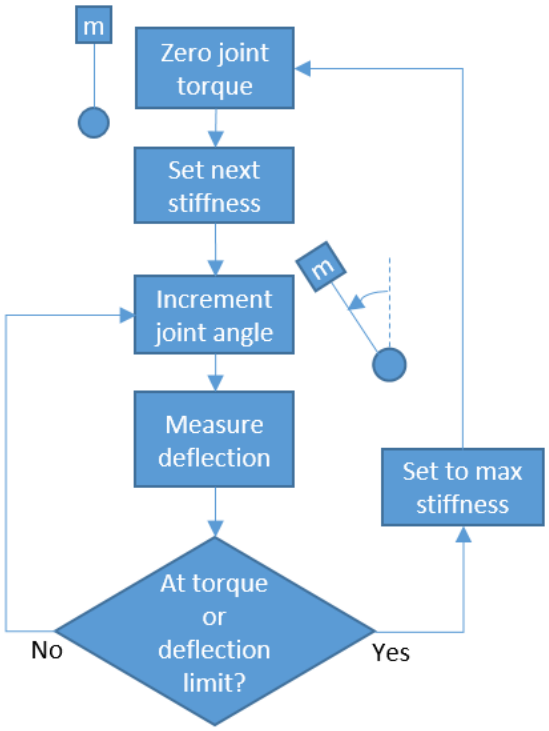

Figure B.1: Sequence of operations for gathering data to calculate joint stiffness.

The deflection was measured for increasing torque loading where initial torque is zero and small moves are made to increase the torque load. Once the maximum testing torque load is reached, small movements are made which decrease the torque back to zero, again pausing along the way to measure deflection. This procedure was repeated for a range of contactor positions. The deflection vs. torque data for each contactor position was then fit using linear regression. The slope of the best fit line is taken to be the stiffness of the joint for that contactor position. Compiling the stiffness calculated in this

way for each joint gives the stiffness vs. contactor position data shown below in Figure B.2, Figure B.3, and Figure B.4

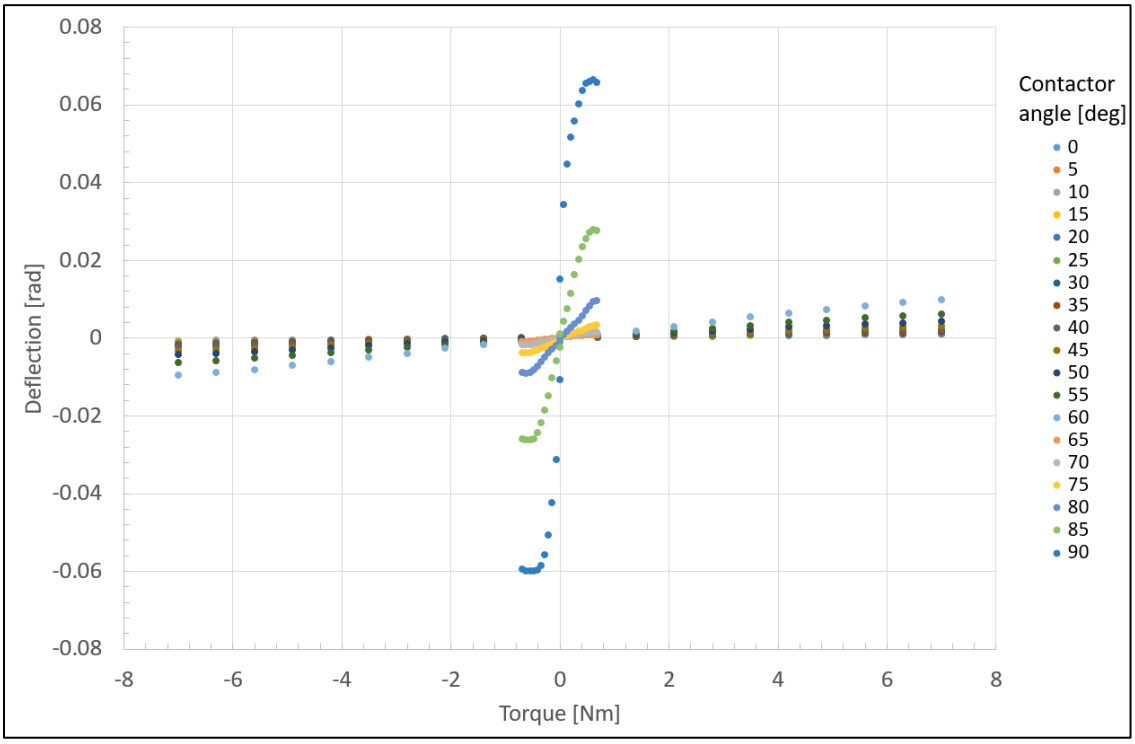

Figure B.2: Shoulder stiffness calibration measurement data. Deflection is recorded over the range of contactor positions and applied torque.

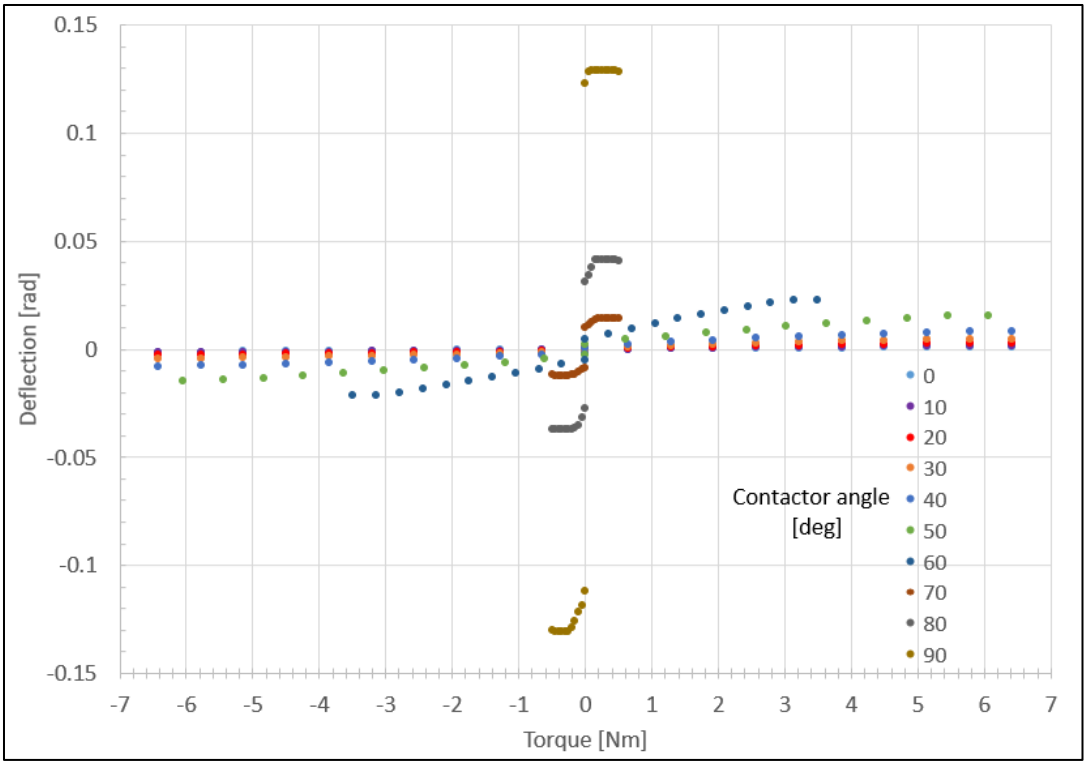

Figure B.3: Elbow joint stiffness calibration measurement data. Deflection is recorded over the range of contactor positions and applied torque.

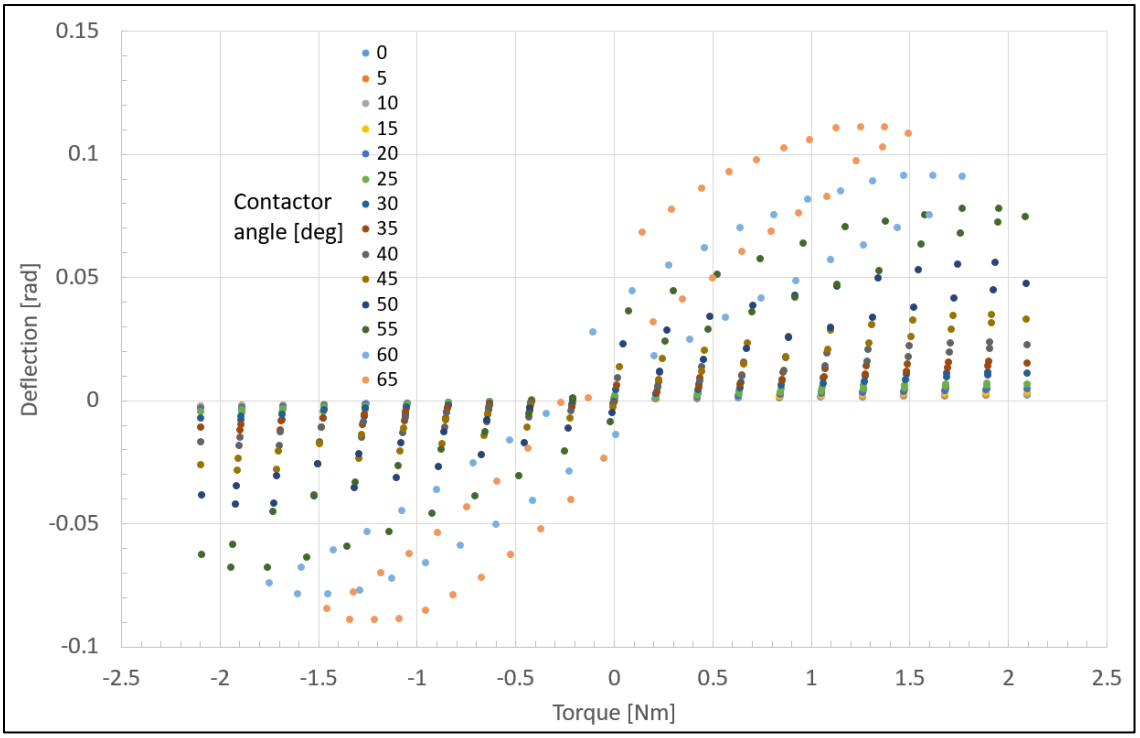

Figure B.4: Wrist stiffness calibration measurement data. Deflection is recorded over the range of contactor positions and applied torque.

Appendix C BILL OF MATERIALS

A materials cost summary is given below for the full robot system.

Table C-1: Robot system cost summary

Electrical Subtotal	$24,081.35
Mechanical Subtotal	$1,692.10
Machined to Print Subtotal	$12,942.12
Total Cost	**$38,715.57**

Detailed bills of material for the project are given below for electrical, mechanical, and machined parts.

Table C-2: Electrical Bill of Materials

P/N	Description	Manufacturer/ Source	Price/Ea.	Qty.	Ext. Price
AKD-P00306-NBCC-0000	AC Servo Drive	Kollmorgen	$799.00	3	**$2,397.00**
P-AKD-CAN-TERM	CAN network termination	Kollmorgen	$14.45	1	**$14.45**
FHA-8C-100-US200	Wrist Harmonic Drive Actuator	Harmonic Drives	$1,785.00	1	**$1,785.00**
FHA-14C-100-US200	Elbow Harmonic Drive Actuator	Harmonic Drives	$2,142.00	1	**$2,142.00**
FHA-17C-160-US250	Shoulder Harmonic Drive Actuator	Harmonic Drives	$2,363.00	1	**$2,363.00**
9105-TIF-DELTA	Delta DAQ F/T Transducer, SI-330-30	ATI Industrial Automation	$5,225.00	1	**$5,225.00**
9105-C-H-PS-5	DAQ F/T transducer cable, Hirose connector to power supply, 5m	ATI Industrial Automation	$310.00	1	**$310.00**
9105-PS-1	DAQ Transducer Power Supply	ATI Industrial Automation	$700.00	1	**$700.00**
9105-C-PS-U-1	Cable from power supply to DAQ Card, unterminated, 1m	ATI Industrial Automation	$155.00	1	**$155.00**
DN-CLIP-FM5-5	DIN RAIL MOUNTING CLIP 5/PK 5mm MOUNTING HOLE FOR 35mm DIN RAIL	Automation Direct	$7.00	1	**$7.00**
DN-R35S1-2	DIN RAIL 35mm x 7.5mm 2/PK 1m (3.3ft) SLOTTED STEEL	Automation Direct	$9.00	1	**$9.00**

AC1-AP-1A	INDUC PROX 4MM SHIELDED PNP .8mm RNG, N.O. PIGTAIL 6.5FT(2M)	Automation Direct	$22.50	3	**$67.50**
AE1-AP-1A	INDUC PROX 8mm SHIELDED PNP 1.5mm RNG 3-WIRE 10-30VDC N.O. PIGTAIL 6.5ft/2m	Automation Direct	$21.00	2	**$42.00**
PD1-AP-1A	INDUC PROX 5mm SHIELDED PNP 0.8mm RNG 3-WIRE 10-30VDC N.O. PIGTAIL 6.5ft/2m	Automation Direct	$41.00	2	**$82.00**
T1E-1015W-1	WIRE DUCT, 1.0 x 1.5 IN., 1/PK, WHT, THIN FINGER, 2M, WITH COVER	Automation Direct	$15.00	1	**$15.00**
DN-R15S1-2	DIN RAIL 15mm x 5.5mm 2/PK 1m (3.3ft) SLOTTED STEEL	Automation Direct	$8.00	1	**$8.00**
KN-10JM12	JUMPER 5/PK 10-POLE FOR KN-M12 OR KN-T12SP4 SERIES PUSH-IN	Automation Direct	$8.50	1	**$8.50**
KN-ECMGRY-10	END COVER 10/PK GRY FOR KN-M12 & KN-M10 SERIES	Automation Direct	$4.00	1	**$4.00**
KN-3JM12	JUMPER 20/PK 3-POLE FOR KN-M12 OR KN-T12SP4 SERIES PUSH-IN	Automation Direct	$7.50	1	**$7.50**
KN-2JM12	JUMPER 25/PK 2-POLE FOR KN-M12 OR KN-T12SP4 SERIES PUSH-IN	Automation Direct	$6.50	1	**$6.50**
KN-4JM12	JUMPER 15/PK 4-POLE FOR KN-M12 OR KN-T12SP4 SERIES PUSH-IN	Automation Direct	$7.50	1	**$7.50**
ECX1651	LEGEND PLATE "EMERGENCY STOP OVERSIZED BLK TXT YEL PLAS FOR 22mm PB	Automation Direct	$2.75	1	**$2.75**
GCX3131	PB MUSH 22mm PLAS RED N.C. TWST-REL 40mm HEAD PLAS BEZEL	Automation Direct	$9.25	1	**$9.25**
BMX-13-W	CABLE GLAND PG11 5-10MM CABLE, 5/PK	Automation Direct	$2.00	1	**$2.00**
MTW20WH	MTW WIRE 20AWG 600V, 500FT, WHITE	Automation Direct	$25.00	1	**$25.00**

MTW20BL	MTW WIRE 20AWG 600V, 500FT, BLUE	Automation Direct	$25.00	1	**$25.00**
RHC242008	ENCLOSURE NEMA 1/3R, 24X20X8IN, STEEL	Automation Direct	$235.00	1	**$235.00**
NP2420PP	SUBPANEL PERF 21x17in FOR 24x20in WALL -MNT MULTI NEMA RATED 14GA STEEL	Automation Direct	$45.00	1	**$45.00**
BM-B1025	CABLE TIE, 100/PK, 18 LB, 4 IN LONG, NATURAL, NYLON 6.6	Automation Direct	$2.00	1	**$2.00**
BM-1100	CABLE TIE INSTALL TOOL,0.098-0.189 IN. WIDE CABLE TIES	Automation Direct	$28.00	1	**$28.00**
BM-B0901	CABLE TIE MOUNT, 100/PK, 3/4 X 3/4 IN, NATURAL NYLON 6.6, ADHESIVE MOUNT	Automation Direct	$7.75	1	**$7.75**
BMX-16-W	CABLE GLAND PG21 13-18MM CABLE, 5/PK	Automation Direct	$4.00	1	**$4.00**
BMX-17-W	CABLE GLAND PG29 18-25MM CABLE, 5/PK	Automation Direct	$7.50	1	**$7.50**
MTW18BK	WIRE MTW 18AWG BLK 500ft SPOOL 600V 16-STRAND BARE COPPER	Automation Direct	$35.00	1	**$35.00**
MTW18RD	WIRE MTW 18AWG RED 500ft SPOOL 600V 16-STRAND BARE COPPER	Automation Direct	$35.00	1	**$35.00**
7000-12741-0000000	FIELD WIREABLE CONNECTOR M12 BARREL 4-PIN MALE AXIAL 18 AWG	Automation Direct	$7.00	3	**$21.00**
7000-12901-0000000	FIELD WIREABLE CONNECTOR M12 NUT 4-PIN FEMALE AXIAL 18 AWG	Automation Direct	$7.00	3	**$21.00**
KN-M12GRY	TERM BLK 100/PK MINI GRY 20A 26-12AWG KONNECT-IT	Automation Direct	$36.00	1	**$36.00**
KN-L5-BLANK-250	MARKING TAG (BLANK) 250/PK 5x5mm	Automation Direct	$7.00	1	**$7.00**
455-2652-1-ND	CONN FEMALE CONTACT 22-28AWG	Digikey	$0.08	25	**$1.93**

455-2654-ND	CONN PLUG HSNG 2POS 2.5MM RED	Digikey	$0.19	10	**$1.89**
455-2653-ND	CONN RCPT HSNG 2POS 2.5MM RED	Digikey	$0.21	10	**$2.09**
455-1909-1-ND	CONN PIN 22-28AWG TIN CRIMP	Digikey	$0.08	25	**$2.01**
AE10G-10-ND	CBL RIBN 10COND 0.050 GRAY 10'	Digikey	$5.27	1	**$5.27**
MPK10K-ND	PLUG CONNECTOR 10 POS W/O FLANGE	Digikey	$4.05	2	**$8.10**
MPL10K-ND	PLUG CONNECTOR 10 POS W/FLANGE	Digikey	$4.05	2	**$8.10**
ED10500-ND	CONN SOCKET IDC 10POS W/KEY GOLD	Digikey	$0.32	2	**$0.64**
817-1915-ND	PWR ENT MOD RCPT IEC320-C14 PNL	Digikey	$24.57	1	**$24.57**
507-1303-ND	FUSE CERAMIC 10A 125VAC 5X20MM	Digikey	$0.28	5	**$1.41**
E2034S-41-50-ND	CABLE 4COND 18AWG GRY SHLD 50'	Digikey	$26.45	1	**$26.45**
BEL1363-100-ND	MULTI-PAIR 6COND 22AWG GRY 100'	Digikey	$58.65	1	**$58.65**
277-2677-ND	CONN D-SUB RCPT 25POS PNL MNT	Digikey	$45.72	1	**$45.72**
626-2113-ND	SCREW LOCK SET 4-40 TYPE 3	Digikey	$0.39	12	**$4.68**
AE1379-ND	CABLE DB9M-DB9F 2M	Digikey	$3.74	4	**$14.96**
209FE-ND	CONN DSUB RCPT 9POS STR SLDR CUP	Digikey	$0.87	3	**$2.61**
CS-DSDHD15MM0-005-ND	DELUXE HD15 M/M 5'	Digikey	$11.55	6	**$69.30**
SFSO4401NR-ND	FEMALE SCREWLOCK 4-40 .312"	Digikey	$0.28	20	**$5.60**
380-1237-ND	CONN MOD PLUG 6P6C UNSHIELDED	Digikey	$0.27	25	**$6.68**
WM9168CT-ND	CONN TERM FEMALE 26-30AWG TIN TR	Digikey	$0.09	50	**$4.32**
WM1837CT-ND	CONN TERM FEMALE 20-24AWG TIN	Digikey	$0.09	50	**$4.34**
WM1784-ND	CONN RECEPT 4POS 3MM VERT DUAL	Digikey	$0.40	5	**$2.00**
WM2490-ND	CONN RECEPT 16POS 3MM DUAL ROW	Digikey	$0.91	4	**$3.64**
WM13070CT-ND	MICROFIT CRIMP TERMINAL 18 AWG	Digikey	$0.10	25	**$2.52**
S9306-ND	CONN SOCKET IDC 10POS W/STR GOLD	Digikey	$0.71	6	**$4.26**

AE10G-25-ND	CBL RIBN 10COND 0.050 GRAY 25'	Digikey	$10.52	1	**$10.52**
S120HCT-ND	RES 120 OHM 1/2W 5% CF MINI	Digikey	$0.10	2	**$0.20**
BKEXP-355-ND	470 TIE POINT 4 BUS STRIPS 8 MOU	Digikey	$7.20	1	**$7.20**
1597-1268-ND	MINI BREAD BOARD 4.5X3.5CM-WHITE	Digikey	$3.01	1	**$3.01**
377-1088-ND	BOX ALUM NAT 3.25"L X 2.13"W	Digikey	$6.30	1	**$6.30**
TL871-ND	CABLE IEC TO NEMA	Digikey	$8.74	1	**$8.74**
SC1554-ND	CONN DSUB 15PIN FMAL-FMAL NICKEL	Digikey	$15.03	3	**$45.09**
609-4045-ND	CONN D-SUB HD RCPT 15POS STR	Digikey	$1.02	4	**$4.08**
277-5346-ND	PWR ENT RCPT NEMA5-15 DIN SCREW	Digikey	$23.20	1	**$23.20**
B78A682B4EE5	DCX22L+GPX22C+ENX16EASY	Maxon	$398.65	1	**$398.65**
709-EDR120-24	DIN Rail Power Supplies 150W 24V 5A EN55022 Class A	Mouser	$24.54	1	**$24.54**
108-DRC-5V10W1AZ	DIN Rail Power Supplies 5V 10W DIN Rail Isolation Class II	Mouser	$18.31	1	**$18.31**
636-973-009-010R011	D-Sub Backshells 9P TOP ENTRY BLACK PLASTIC	Mouser	$3.72	6	**$22.32**
783831-01	cRIO-9064, 4-Slot Integrated Dual-Core Controller, Artix-7 FPGA	National Instruments	$1,799.10	1	**$1,799.10**
779019-01	NI 9912 DIN Rail Mount Kit for 4-slot cRIO/cDAQ Chassis.	National Instruments	$28.80	1	**$28.80**
781673-01	NI 9881, C Series CANopen Interface, 1 Port	National Instruments	$576.90	1	**$576.90**
779519-01	NI 9205 32-Channel ±10 V, 250 kS/s, 16-Bit Analog Input Module	National Instruments	$810.00	1	**$810.00**
779351-01	NI 9401 8-Channel, 100 ns, TTL Digital Input/Output Module	National Instruments	$271.80	1	**$271.80**
N/A	Shipping and Handling	National Instruments	$24.06	1	**$24.06**
MHA7DCH19BT10A00	AKSIM H 19B BISS-C LOW 1M TSHAPE 9 PIN	Renishaw	$337.53	3	**$1,012.59**
MRA7D049AA025B00	AKSIM RING TYPE 7 OD 49 MM ID 25MM	Renishaw	$128.92	3	**$386.76**

HEDM-5500-J12	Incremental Encoder	Avago	$35.44	1	**$35.44**
HEDS-8902	Encoder Cable	Avago	$8.80	1	**$8.80**
784213-3502	NI Academic Site License - LabVIEW Research Only 1 user	National Instruments	$2,339.00	1	**$2,339.00**
Total:					**$24,081.35**

Table C-3: Mechanical components Bill of Materials

Vendor P/N	Description	Manufacturer/ Source	Price/Ea.	Qty	Ext. Price
U-SFAD0.50-L2.24-F0.38-B0.28-T0.38-U0.25-PC-SC0	Linear Shaft	Misumi	$20.11	1	**$20.11**
CSPCSZ-SUS-M5-13	Fully Threaded Phillips Flat Head Screw	SUNCO/Misumi	$0.12	12	**$1.44**
CSPCSZ-SUS-M5-10	Fully Threaded Phillips Flat Head Screw	SUNCO/Misumi	$0.12	12	**$1.44**
CSPCSZ-SUS-M3-7	Fully Threaded Phillips Flat Head Screw	SUNCO/Misumi	$0.07	12	**$0.84**
SFRES10-15-F18.8-P8-T7-S5-Q6-SC2-QC-CKC	Rotary Shafts - Both Ends Stepped, One End Threaded	Misumi	$22.16	3	**$66.48**
SSHC-SUS-M2.5-3	Hex Socket Set Screw - Cup Point	SUNCO/Misumi	$0.21	6	**$1.26**
GEABB0.5-20-3-B-4	Spur Gears - Pressure Angle 20Deg., Module 0.5	Misumi	$8.72	3	**$26.16**
HCDG4-15	Precision Pivot Pins - Flanged, Retaining Ring	Misumi	$2.71	3	**$8.13**
CIMRS12-15-0.3	Shim Rings - Standard	Misumi	$0.67	4	**$2.68**
FL6701ZZ	Small Deep Groove Ball Bearings - Double Shielded with Flanged	Misumi	$11.27	3	**$33.81**
U-CCGH0.19-L0.539	Precision Pivot Pins - Straight, Retaining Ring Grooves, Configurable (INCH)	Misumi	$10.20	12	**$122.40**
9016403	1/4 Inch Bore Diameter, 360 Lb. Dynamic Load Capacity, 1/4 x 7/16 x 1/4 Inch, Caged, Open End, Shell Needle Roller Bearing – 7/16 Inch Outside Diameter, 1/4 Inch Wide	IKO/MSC Direct	$15.47	12	**$185.64**

9016387	3/16 Inch Bore Diameter, 400 Lb. Dynamic Load Capacity, 3/16 x 11/32 x 1/4 Inch, Caged, Open End, Shell Needle Roller Bearing – 11/32 Inch Outside Diameter, 1/4 Inch Wide	INA Bearing/ MSC Direct	$13.94	12	**$167.28**
93574A207	18-8 Stainless Steel Shims for Spacing 5/64" and 1/8" ID Bearings, 0.005" Thick, undefined: undefined, Packs of 25	McMaster-Carr	$9.23	1	**$9.23**
90145A505	18-8 Stainless Steel Dowel Pin 3/16" Diameter, 1/2" Length, Packs of 20	McMaster-Carr	$4.77	1	**$4.77**
92949A816	18-8 SS Hex Drive Rounded Head Screw 6-32 Thread Size, 1-1/8" Long, Packs of 100	McMaster-Carr	$7.88	1	**$7.88**
91443A110	3/16" Lg. Adhesive-Back Unthrd Spacers, Packs of 10	McMaster-Carr	$12.62	1	**$12.62**
8174A45	Precision Needle File Set Economy, 12-Piece, Finish NO. 0, 6-1/4" Long	McMaster-Carr	$20.00	1	**$20.00**
8174A47	Precision Needle File Set Economy, 12-Piece, Finish NO. 4, 6-1/4" Long	McMaster-Carr	$20.00	1	**$20.00**
1244K14	Extendable Spout Oiler with Machine Oil 4-oz Squeeze Bottle, ISO Grade 32, SAE Grade 10W	McMaster-Carr	$3.37	1	**$3.37**
8511A11	Press-Fit Fixture Support 1/4" Diameter, 1/4" Long	McMaster-Carr	$2.01	2	**$4.02**
8511A17	Press-Fit Fixture Support 1/4" Diameter, 1/8" Long	McMaster-Carr	$3.97	1	**$3.97**
57155K301	Stainless Steel Ball Bearing Open Flanged, for 3/16" Shaft Dia, 3/8" OD	McMaster-Carr	$6.97	24	**$167.28**
7804K145	Stainless Steel Ball Bearing Flanged Dbl Shielded, for 8 mm Shaft Dia, 12 mm OD	McMaster-Carr	$7.77	3	**$23.31**

90145A436	18-8 Stainless Steel Dowel Pin 3/32" Diameter, 3/8" Length, Packs of 100	McMaster-Carr	$12.47	1	**$12.47**
90145A434	18-8 Stainless Steel Dowel Pin 3/32" Diameter, 1/4" Length, Packs of 100	McMaster-Carr	$11.13	1	**$11.13**
91292A112	18-8 Stainless Steel Socket Head Screw M3 X 0.5 mm Thread, 8 mm Long, Packs of 100	McMaster-Carr	$4.00	1	**$4.00**
92000A100	18-8 SS Phillips Rounded Head Screws M2.5 X 0.45 mm Thread, 3 mm Long, Packs of 100	McMaster-Carr	$4.48	1	**$4.48**
91290A021	Black-Oxide Alloy Steel Socket Head Screw M1.6 X 0.35 mm Thread, 4 mm Long, Packs of 25	McMaster-Carr	$3.11	1	**$3.11**
91102A715	Zinc-Plated Steel Split Lock Washer for NO. 3 Screw Size, 0.107" ID, 0.195" OD, Packs of 100	McMaster-Carr	$1.14	1	**$1.14**
91251A094	Black-Oxide Alloy Steel Socket Head Screw 3-48 Thread Size, 3/8" Long, Packs of 100	McMaster-Carr	$6.22	1	**$6.22**
92196A145	18-8 Stainless Steel Socket Head Screw 6-32 Thread Size, 5/16" Long, Packs of 100	McMaster-Carr	$4.68	1	**$4.68**
91771A191	18-8 SS Phillips Flat Head Screws 8-32 Thread Size, 5/16" Long, Packs of 100	McMaster-Carr	$5.80	1	**$5.80**
91124A059	Spring Steel Shim for Shortening Screw Shldrs 0.010" Thick, for 1/4" Shoulder Dia, 0.250" ID, Packs of 25	McMaster-Carr	$4.70	1	**$4.70**
92414A009	Steel Unthreaded Spacer 1/8" OD, 1/4" Lg., for NO. 0 Screw Sz	McMaster-Carr	$1.26	24	**$30.24**
91771A057	18-8 SS Phillips Flat Head Screws 0-80 Thread Size, 3/8" Long, Packs of 100	McMaster-Carr	$9.44	1	**$9.44**

97633A120	Black-Finish Steel External Retaining Ring for 3/16" Shaft Diameter, Packs of 100	McMaster-Carr	$7.82	1	**$7.82**
99040A950	Type 18-8 Stainless Steel Shim for Shafts 0.014" Thick, 0.063" ID, 0.156" OD, Packs of 25	McMaster-Carr	$9.86	1	**$9.86**
92146A540	18-8 Stainless Steel Split Lock Washer for NO. 6 Screw Size, 0.148" ID, 0.25" OD, Packs of 100	McMaster-Carr	$1.53	1	**$1.53**
93615A218	18-8 SS Low-Profile Sckt Head Screws 6-32 Thread Size, 5/8" Long, Packs of 25	McMaster-Carr	$10.42	1	**$10.42**
90309A340	Brass Unthreaded Spacer 1/2" OD, 1/8" Lg., for 1/4" Screw Sz	McMaster-Carr	$1.78	6	**$10.68**
94355A140	Nonmarring Flat Point Socket Set Screw 18-8 Stainless Steel, 4-40 Thread, 1/4" Long, Packs of 50	McMaster-Carr	$4.44	1	**$4.44**
2685T13	Ultra-Low-Friction Dry-Running Sleeve Bearing PTFE, for 10mm Shaft Dia	McMaster-Carr	$3.97	1	**$3.97**
91290A041	Black-Oxide Alloy Steel Socket Head Screw, M1.6 x 0.35 mm Thread, 8 mm Long	McMaster-Carr	$3.10	1	**$3.10**
92146A510	18-8 Stainless Steel Split Lock Washer for Number 0 Screw Size, 0.062" ID, 0.137" OD	McMaster-Carr	$3.93	1	**$3.93**
26015A632	Tap M1.6 x 0.35 mm Thread	McMaster-Carr	$13.05	1	**$13.05**
RA035XP0	4-Point Contact Bearing Type X with 3.5 inch Bore Slim Section	Kaydon	$84.99	1	**$84.99**
KA-035-XP0	4-Point Contact Bearing Type X with 3.5 inch Bore Slim Section	Kaydon	$111.79	2	**$223.58**
A 1B 3MYK05040	1:2 Ratio / 0.5 MOD Bevel Gear 40 tooth	SDP-SI	$36.71	3	**$110.13**
A 1B 3MYK05020	1:2 Ratio / 0.5 MOD Bevel Gear 20 tooth	SDP-SI	$19.38	3	**$58.14**
11M181	Headless Press Fit Drill Bushing, 1/2" OD	Grainger	$1.64	1	**$1.64**

11N430	Slip Fixed Renewable Combination Drill Bushing, 1/2" ID, 1" OD	Grainger	$2.82	1	**$2.82**
18f.5x8-18	1/2" x 8" x 18" 1018 Steel Flat, Cold Finished	Speedy Metals	$47.12	1	**$47.12**
18f.5x5	1/2" x 5" x 5" 1018 Steel Flat, Cold Finished	Speedy Metals	$7.85	1	**$7.85**
18f.125x1.5	1/8" x 1-1/2" x 2-1/2" 1018 Steel Flat, Cold Finished	Speedy Metals	$0.66	2	**$1.32**
18f.5x1.5	1/2" x 1-1/2" x 7" 1018 Steel Flat, Cold Finished	Speedy Metals	$3.15	2	**$6.30**
18f.5x1.5	1/2" x 1-1/2" x 1-1/4" 1018 Steel Flat, Cold Finished	Speedy Metals	$0.90	2	**$1.80**
18f1.5x5	1-1/2" x 5" x 4-1/16" 1018 Steel Flat, Cold Finished	Speedy Metals	$26.35	2	**$52.70**
18f1x4	1" x 4" x 6" 1018 Steel Flat, Cold Finished	Speedy Metals	$13.38	1	**$13.38**
Total:					**$1,692.10**

Table C-4: Machined Parts bill of materials for robot system.

P/N	Description	Price/Ea.	Qty	Ext. Price
VSA00-01	BASE PLATE	*	1	*
VSA01-01	SHOULDER FLEXURE	$295.00	2	**$590.00**
VSA01-02	DRIVE FLANGE	$325.00	3	**$975.00**
VSA01-03	OUTPUT CUP	$340.00	3	**$1,020.00**
VSA01-04	BOTTOM PLATE	$125.00	3	**$375.00**
VSA01-05	CONTACTOR PRIMARY DRIVE SHAFT	$55.00	12	**$660.00**
VSA01-06	ELBOW FLEXURE	$255.00	2	**$510.00**
VSA01-07	RING GEAR LOWER	$425.00	3	**$1,275.00**
VSA01-08	RING GEAR UPPER	$405.00	3	**$1,215.00**
VSA01-09	WRIST FLEXURE	$275.00	2	**$550.00**
VSA01-11	CARRIER ARM BODY	$35.00	12	**$420.00**
VSA01-12	CARRIER ARM COVER	$35.00	9	**$315.00**
VSA01-14	INPUT CUP BEARING COVER	$75.00	3	**$225.00**
VSA01-17	CENTER TRANSFER GEAR	$80.00	3	**$240.00**
VSA01-18	CONTACTOR DRIVE GEAR	$31.00	12	**$372.00**
VSA01-19	SUN GEAR	$28.00	24	**$672.00**
VSA01-20	PLANET GEAR	$28.00	24	**$672.00**
VSA01-21	ENCODER HUB	$140.00	3	**$420.00**
VSA01-22	HOMING CARRIER ARM COVER	$85.00	3	**$255.00**

VSA01-23	CONTACTOR MOTOR MOUNT	$98.00	3	**$294.00**
VSA01-24	SECONDARY CONTACTOR DRIVE GEAR	$31.00	6	**$186.00**
VSA01-25	DCX22 Motor Mount	$111.87	2	**$223.74**
VSA03-01	HUMERUS LINK	$431.98	1	**$431.98**
VSA03-02	FOREARM LINK	$587.38	1	**$587.38**
VSA03-03	HAND	$208.02	1	**$208.02**
VSA04-02	CRANK ARM	*	1	*
VSA04-04	LEAD SCREW BEARING BLOCK	*	1	*
VSA04-05	FORCE SENSOR ADAPTER PLATE	*	1	*
VSA04-06	BASE JOINT MOUNT	$250.00	1	**$250.00**
VSA04-07	BASE SLIDE	*	1	*
VSA04-08	CRANK BEARING BLOCK	*	1	*
VSA04-09	CRANK SHAFT	*	1	*
VSA04-10	REAR CRANK BEARING BLOCK	*	1	*
VSA04-11	CRANK ENCODER BRACKET	*	1	*
VSA04-12	ATI DELTA TOOLING ADAPTER PLATE	*	1	*
VSA06-01	TEST LOAD	*	1	*
			Total:	**$12,942.12**

** Components machined at Marquette's Discovery Learning Lab. Materials cost is included in Mechanical components cost summary.*